AFRL-PR-WP-TR-2001-2041

THERMAL MANAGEMENT RESEARCH STUDIES

VOLUME 1: HIGH PERFORMANCE MINIATURE HEAT PIPES

LANCHAO LIN, Ph.D.
UES, INC.
4401 DAYTON-XENIA ROAD
DAYTON, OH 45432-1894

RENGASAMY PONNAPPAN, Ph.D.
AFRL/PRPS
1950 FIFTH STREET
BUILDING 18, ROOM G041A
WRIGHT-PATTERSON AFB, OH 45433-7251

MARCH 2001

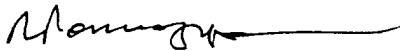**FINAL REPORT FOR PERIOD 20 AUGUST 1996 – 31 DECEMBER 2000**

20010515 019

PROPULSION DIRECTORATE
AIR FORCE RESEARCH LABORATORY
AIR FORCE MATERIEL COMMAND
WRIGHT-PATTERSON AIR FORCE BASE, OH 45433-7251

NOTICE

USING GOVERNMENT DRAWINGS, SPECIFICATIONS, OR OTHER DATA INCLUDED IN THIS DOCUMENT FOR ANY PURPOSE OTHER THAN GOVERNMENT PROCUREMENT DOES NOT IN ANY WAY OBLIGATE THE US GOVERNMENT. THE FACT THAT THE GOVERNMENT FORMULATED OR SUPPLIED THE DRAWINGS, SPECIFICATIONS, OR OTHER DATA DOES NOT LICENSE THE HOLDER OR ANY OTHER PERSON OR CORPORATION; OR CONVEY ANY RIGHTS OR PERMISSION TO MANUFACTURE, USE, OR SELL ANY PATENTED INVENTION THAT MAY RELATE TO THEM.

THIS REPORT IS RELEASABLE TO THE NATIONAL TECHNICAL INFORMATION SERVICE (NTIS). AT NTIS, IT WILL BE AVAILABLE TO THE GENERAL PUBLIC, INCLUDING FOREIGN NATIONS.
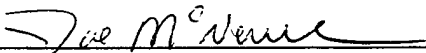
THIS TECHNICAL REPORT HAS BEEN REVIEWED AND IS APPROVED FOR PUBLICATION.

RENGASAMY PONNAPPAN
Senior Mechanical Engineer
Energy Storage & Thermal Sciences Branch

BRIAN G. HAGER
Chief
Energy Storage & Thermal Sciences Branch

JOE MCNAMEE, Major, USAF
Deputy Chief
Power Division

Do not return copies of this report unless contractual obligations or notice on a specific document requires its return.

REPORT DOCUMENTATION PAGE		Form Approved OMB No. 074-0188

Public reporting burden for this collection of information is estimated to average 1 hour per response, including the time for reviewing instructions, searching existing data sources, gathering and maintaining the data needed, and completing and reviewing this collection of information. Send comments regarding this burden estimate or any other aspect of this collection of information, including suggestions for reducing this burden to Washington Headquarters Services, Directorate for Information Operations and Reports, 1215 Jefferson Davis Highway, Suite 1204, Arlington, VA 22202-4302, and to the Office of Management and Budget, Paperwork Reduction Project (0704-0188), Washington, DC 20503

1. AGENCY USE ONLY (Leave blank)	2. REPORT DATE March 2001	3. REPORT TYPE AND DATES COVERED Final, 08/20/1996 – 12/31/2000

4. TITLE AND SUBTITLE Thermal Management Research Studies Volume 1: High Performance Miniature Heat Pipes	5. FUNDING NUMBERS C: F33615-96-C-2680 PE: 62203F PN: 3145 TN: 20 WU: C4
6. AUTHOR(S) Lanchao Lin, Ph.D. Rengasamy Ponnappan, Ph.D.	

7. PERFORMING ORGANIZATION NAME(S) AND ADDRESS(ES)		8. PERFORMING ORGANIZATION REPORT NUMBER
UES, INC. 4401 DAYTON-XENIA ROAD DAYTON, OH 45432-1894	AFRL/PRPS 1950 FIFTH STREET BUILDING 18, ROOM G041A WRIGHT-PATTERSON AFB, OH 45433-7251	UES-P155-01-001 (Vol. 1)

9. SPONSORING / MONITORING AGENCY NAME(S) AND ADDRESS(ES)	10. SPONSORING / MONITORING AGENCY REPORT NUMBER
PROPULSION DIRECTORATE AIR FORCE RESEARCH LABORATORY AIR FORCE MATERIEL COMMAND WRIGHT-PATTERSON AIR FORCE BASE, OH 45433-7251 POC: RENGASAMY PONNAPPAN, AFRL/PRPS, (937) 255-2922	AFRL-PR-WP-TR-2001-2041

11. SUPPLEMENTARY NOTES: The other volume of this report is: Thermal Management Research Studies, Volume 2: Experimental Investigation of Oscillating Heat Pipes for Actuator Cooling. (AFRL-PR-WP-TR-2001-2042)

12a. DISTRIBUTION / AVAILABILITY STATEMENT Approved for public release; distribution unlimited.	12b. DISTRIBUTION CODE

13. ABSTRACT (Maximum 200 Words)

High performance miniature heat pipes are developed for the cooling of high heat flux electronics using new capillary structures which rely on the use of a folded copper sheet fin and a folded copper screen. Using the folded sheet fin, capillary fins with fully opened grooves and folded sheet fins with notches at the fin top are made through a brazing process and the electric-discharge-machining technique. The use of the folded screen simplifies the heat pipe fabrication process. It is easy to make the capillary grooves as dense as desired through the present fabrication techniques. Heat pipes with different capillary structures and fill amounts are tested in the horizontal orientation. Three different heating areas in the heat pipe evaporator are arranged by activating different numbers of chip resistors. Thermal performances of the heat pipes are compared. The heat pipe with notched fins has the lowest internal thermal resistance at similar operating temperatures. In general, the heat pipes with notched fins, capillary fins and a folded screen demonstrated their favorable thermal performance. Compared with the capillary fins, the use of the folded sheet fins with notches resulted in a significant increase in the condenser heat transfer coefficient by 120 percent or greater at an operating temperature of 110 °C. Heat fluxes higher than 140 W/cm2 are achieved using one-chip and two-chip heating modes.

14. SUBJECT TERMS Electronics cooling, miniature heat pipe, capillary fin, folded sheet fin, folded screen, notched fin, maximum performance, evaporator heat transfer coefficient, condenser heat transfer coefficient, heat transfer enhancement.	15. NUMBER OF PAGES 86
	16. PRICE CODE

17. SECURITY CLASSIFICATION OF REPORT Unclassified	18. SECURITY CLASSIFICATION OF THIS PAGE Unclassified	19. SECURITY CLASSIFICATION OF ABSTRACT Unclassified	20. LIMITATION OF ABSTRACT SAR

| NSN 7540-01-280-5500 | | | Standard Form 298 (Rev. 2-89)
Prescribed by ANSI Std. Z39-18
298-102 |

TABLE OF CONTENTS

TABLE OF CONTENTS (CONT'D.)

LIST OF FIGURES

LIST OF FIGURES (CONT'D.)

LIST OF TABLES

NOMENCLATURE

A_e	effective heating area
A_c	cooling area
A_h	heating area
A_l	cross-sectional area of liquid flow per groove
A_v	cross-sectional area of vapor flow
B_f	length of fin area (see Figure 2.3)
B_l	vapor core width
Bo	Bond number, $D_{h,v}[g(\rho_l - \rho_v)/\sigma]^{0.5}$
C	ratio of vapor core height to width
C_k	parameter
D_h	hydraulic diameter
f	friction coefficient
g	gravitational constant
h_c	condenser heat transfer coefficient
h_e	evaporator heat transfer coefficient
h_{fg}	latent heat of vaporization
H_f	fin height
H_l	vapor core height
I	electric current
k	thermal conductivity
k_{eff}	effective thermal conductivity of saturated fin
L	length
L_{eff}	heat pipe effective length
N	total fin number
Δp_c	capillary pressure
q_e	evaporator heat flux
Q	total heat rate

Q_b boiling limit

Q_c capillary limit

Q_e entrainment limit

Q_{bot} heat rate through bottom cooler

Q_{in} input power

Q_{loss} heat losses

Q_s sonic limit

Q_{top} heat rate through top cooler

R_n bubble size of nucleate boiling

R_v gas constant of vapor

Re   Reynolds number, $D_h u \rho / \mu$

t_i average groove depth

t_s groove depth

t_w heat pipe wall thickness

T   heat pipe wall temperature

T_v heat pipe operating temperature

ΔT_{ec} average evaporator-to-condenser temperature difference

u   velocity

V   voltage

W   groove width

γ ratio of specific heats

δ fin width

θ_f contact angle between a solid-liquid interface and a liquid-vapor interface

θ_w contact angle between a saturated screen surface and a liquid-vapor interface

θ_0 minimum wetting contact angle

μ dynamic viscosity

ν kinematic viscosity

ρ density

σ surface tension

ϕ fill ratio

Subscripts

a   adiabatic

c   condenser

e   evaporator

i   inner

l   liquid, bottom surface

m   mean

s   solid

u   top surface

v   vapor

w   saturated screen, wall

FOREWORD

1   INTRODUCTION

Advanced packages of high power electronics for the US Air Force and space related programs require the use of high performance heat transfer elements to remove high heat flux heat from the power electronics. Heat fluxes higher than 100 W/cm^2 are often predicted for the advanced power electronics. Meanwhile, the upper limit of the operating temperature of the power electronics is settled below 120°C[1]. Many practical cooling approaches dealing with subcooled flow boiling in a straight channel, curved channel and channel with discrete heat sources have been studied. Leland has given state-of-the-art assessments in this area[2]. Passive cooling methods using heat pipes have garnered attention due to continuous development in heat pipe theory and application[3,4,5]. Miniature heat pipe (MHP) is one of the promising heat transfer elements capable of dealing with the high heat flux electronics cooling.

Plesch et al. reported their test results of two different MHPs with overall dimensions of 7 mm wide, 2 mm thick and 120 mm long[6]. It was found that the heat pipe with longitudinal grooves had a larger heat transport rate. The maximum heat flux was 35 W/cm^2 and the temperature drop over the heat pipe in this case was about 35°C in the horizontal orientation. Cao et al. tested two MHPs with axial grooves[7]. The heat pipe shell as well as the grooves were fabricated using the electric-discharge-machining (EDM) technology. The depth, width and pitch of the groove for one of their heat pipes were 0.25 mm, 0.1 mm and 0.2 mm. The overall dimensions for the heat pipe were 7 mm wide, 2 mm thick and 80 mm long. The maximum heat input and evaporator heat flux were about 31 W and 20.6 W/cm^2 for the horizontal arrangement. More recently, Faghri and Khrustalev reported that their copper-water MHP with axial rectangular micro capillary grooves could remove heat at heat flux levels of 82 W/cm^2 from a heating area of 1.4 cm^2 and 150W/cm^2 from a heating area of 0.7 cm^2 in the horizontal orientation at an operating temperature of 90°C[8]. To provide a simple and low cost solution to the manufacturing of micro wick structures, Ponnappan investigated a new folded-screen wick, copper-water MHP[9]. It was indicated that on a small heating area of 0.774cm^2, the MHP of this type could handle a heat flux of 115W/cm^2 at the operating temperature of 90°C and evaporator-to-adiabatic temperature difference of 37°C[9]. By comparison of the published results of MHPs[6-9], the MHP with micro capillary grooves (0.2 mm wide by 0.42 mm deep)[8] was superior in

1

the heat transfer characteristic. In spite of the high performance, the evaporator-to-condenser temperature difference of the MHP with micro capillary grooves reached 21°C at 100 W which corresponded to 64 W/cm^2 in the evaporator, indicating that at the high heat flux, the temperature difference between the evaporator and condenser was high.

In order to decrease the evaporator-to-condenser temperature difference of the MHP at high evaporator heat fluxes, several MHPs have been developed at the Air Force Research Laboratory, Wright-Patterson AFB. The MHPs contain new capillary structures made out of a folded copper sheet fin and a folded copper screen. Particularly, a heat transfer enhancement method is developed that deals with using folded copper sheet fins with notches at the fin top as the heat pipe capillary structure. The notches appear only in the evaporator and condenser. The fins are brazed onto either wide side of the MHP. The notches (small holes) let the vapor escape from the groove into the vapor core. As opposed to the notches, the fin bridges (uncut part at the fin top) separating notches at the top of the fins protect the returning liquid against the interfacial shear stress of countercurrent two-phase flow to some extent and consequently reduce the liquid flow resistance. Meanwhile, the fin bridges in the heat pipe condenser serve as additional secondary heat transfer area and contribute to the enhancement of condensation heat transfer.

For closed two-phase thermosyphons, the reduction of the interaction between the vapor flow and liquid flow could be achieved using a perforated tube flow separator[10]. For the present MHP, the copper sheet fin with notches cut functions as two-phase flow separator. The objective of the present study is to compare heat transfer characteristics of the heat pipes with new capillary structures and to verify the heat transfer enhancement method, especially under high heat fluxes.

2

2 PERFORMANCE LIMITATIONS OF MINIATURE HEAT PIPES

Power Division (AFRL/PRP) researchers have developed new fabrication techniques to produce MHPs that have more flexible capillary structures. One basic configuration is a heat pipe with capillary fins on its inner wall. A fin assembly is shown in Figure 2.1. The assembly is made by brazing a folded sheet on the wide side and making a full cut on the top of the fins using EDM technology. Another basic type of capillary structure is a folded screen wrapped around the heat pipe inner wall as shown in Figure 2.2. It is much easy to fabricate the heat pipe with the folded screen installed. Like conventional heat pipes, the operation of a MHP is subject to a number of performance limitations which determine the maximum heat transfer rate of the MHP under certain operating conditions. The type of performance limitation that restricts the operation of a MHP is determined by which limitation has the lowest value at a given heat pipe operating temperature. Most performance limitations of heat pipe depend on types of capillary structures. One of the most commonly used capillary structures is formed by axial grooves. The axially-grooved heat pipe has a similar operating principle to the capillary fin heat pipe. We will first focus on physical phenomena of the maximum performance in the heat pipe with capillary fins. Other new types of capillary structures will then be discussed.

2.1 Performance Limitations of a Heat Pipe with Capillary Fins

The capillary fin is a basic and promising capillary structure of MHP since many advanced composite wicks are associated with the capillary fin. Physical phenomena that might limit the heat transfer in the capillary fin heat pipe are related with four performance limitations such as the capillary limit, entrainment limit, boiling limit and sonic limit. Mathematical relations for prediction of these limitations are presented. Geometric parameters on the cross section of the heat pipe with capillary fins are shown in Figure 2.3.
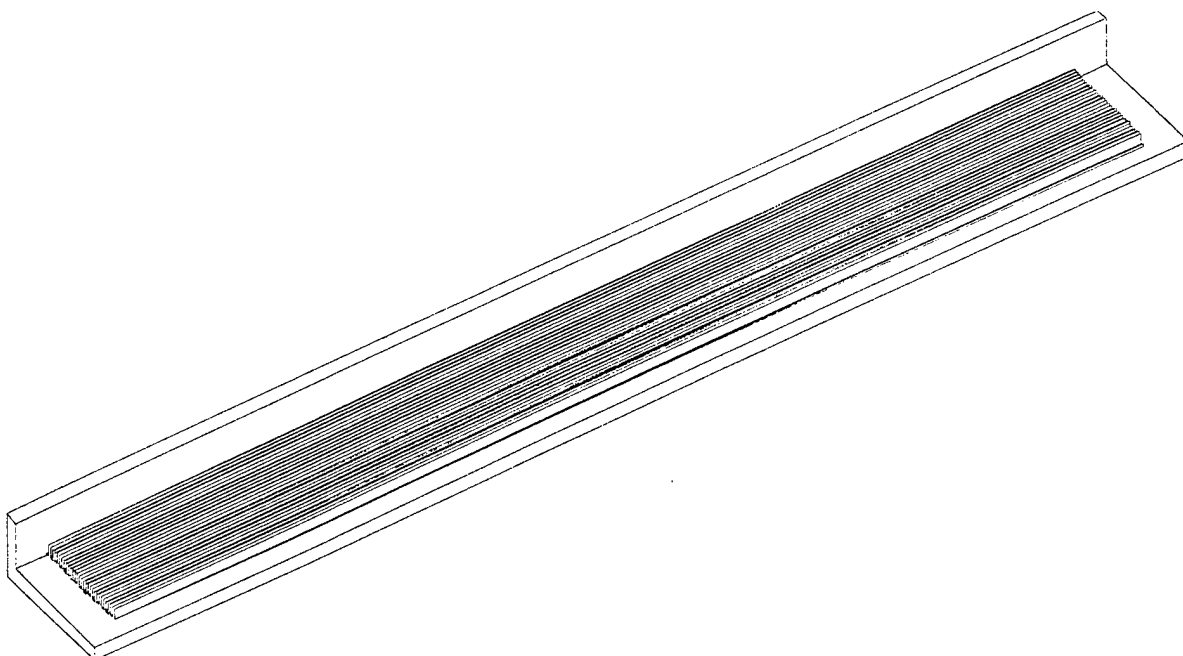
Figure 2.1   3-D view of capillary fins on the wall of MHP
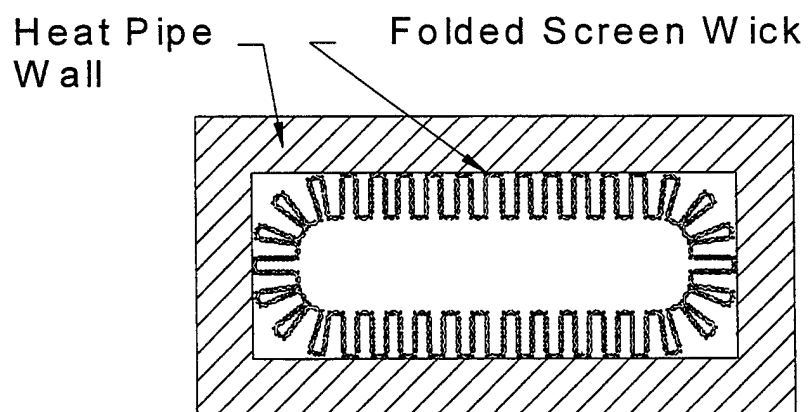
Figure 2.2   Heat pipe with a folded screen.
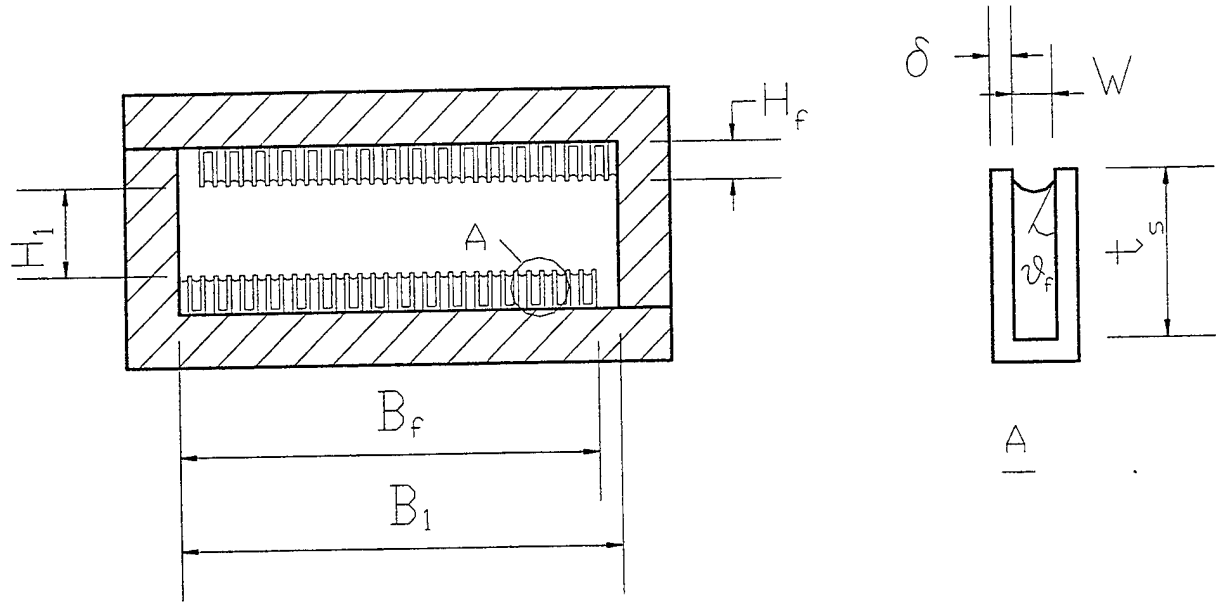
Figure 2.3   Cross-sectional view of a heat pipe with capillary fins.

Capillary limit

The working fluid circulation in the heat pipe is maintained by the capillary pressure head of the capillary structure. The pumping ability of the capillary structure is limited by such a condition that the maximum capillary pressure head can not balance the sum of pressure losses along the vapor-liquid path. The capillary limitation is predicted using relations proposed by Hopkins et al.[11] The geometric parameters of the MHP with rectangular capillary fins are calculated as follows.

The effective length of MHP:

$$L_{eff} = 0.5(L_e + L_c) + L_a \, , \tag{1}$$

where L_e, L_c and L_a are the lengths of evaporator, condenser and adiabatic section.

The cross-sectional area of vapor flow:

$$A_v = B_1 \, H_1 \, . \tag{2}$$

The average liquid depth in the groove:

$$t_l = (t_s + 0.5\delta)\phi \, , \tag{3}$$

5

where ϕ is the ratio of the working fluid fill amount to the volume of all the grooves

The cross-sectional area of liquid flow in one groove:

$$A_l = W\, t_l \,. \tag{4}$$

The effective heating area:

$$A_e = L_e B_f \,. \tag{5}$$

The hydraulic diameter of vapor channel:

$$D_{h,v} = \frac{2\, A_v}{(B_1 + H_1)} \,. \tag{6}$$

The hydraulic diameter of liquid channel:

$$D_{h,l} = \frac{4 A_l}{(W + 2\, t_l)} \,. \tag{7}$$

Friction coefficients for the vapor and liquid flows are calculated using the following correlations. For vapor flow:

$$(fRe)_v = 24(1 - 1.3553C + 1.9467\,C^2 - 1.7012\,C^3 + 0.9564\,C^4 - 0.2537\,C^5)\,, \tag{8}$$

where Re_v is the Reynolds number of vapor and

$$C = \frac{H_1}{B_1} \,. \tag{9}$$

For liquid flow without liquid-vapor interaction:

$$(fRe)_{l0} = 8\,t_l^2 \left[\frac{W^2}{4}(1 + \frac{2\,t_l}{W})^2 (\frac{1}{3} - \frac{32W}{\pi^5\, t_l} \tanh \frac{\pi\, t_l}{W}) \right]^{-1} \,, \tag{10}$$

where "$_0$" is related to zero liquid-vapor interface shear.

For liquid flow with liquid-vapor interaction:

$$(fRe)_l = (fRe)_{l0} \left\{ 1 + \frac{NW^3}{6\pi\, D_{h,v}^3}(fRe)_v \frac{v_v}{v_l} \left[1 - 1.971\exp(-\frac{\pi\, t_l}{W}) \right] \right\} \,, \tag{11}$$

where N is the total fin number, and v_v and v_l are the kinematic viscosities of vapor and liquid.

The capillary pressure is defined as

6

$$\Delta p_c = \frac{2\sigma \cos\theta_0}{W} , \tag{12}$$

where σ is the surface tension and θ_0 the minimum wetting contact angle.

The capillary limitation has the following form.

$$Q_c = \frac{h_{fg}\Delta p_c}{L_{eff}} \left[(fRe)_v \frac{2\mu_v}{D_{h,v}^2 \rho_v A_v} + (fRe)_l \frac{2\mu_l}{D_{h,l}^2 \rho_l N A_l} \right]^{-1} , \tag{13}$$

where h_{fg} is the latent heat of vaporization, ρ_v and ρ_l are the densities of vapor and liquid, and μ_v and μ_l the dynamic viscosities of vapor and liquid.

Entrainment limit

The vapor and liquid flows within a heat pipe are in direct contact with each other and flow in opposite direction. When the vapor velocity in the heat pipe is sufficiently high, the shear force existing at the liquid-vapor interface may tear the liquid from the capillary fin surface and entrain it into the vapor flow stream. This phenomenon reduces the condensate return to the evaporator and limits the heat transport capability. For grooved heat pipes, Tien and Chung[12] proposed a correlation of the entrainment limit which has the following form.

$$Q_e = C_k^2 A_v h_{fg} \left(\frac{\sigma}{W} \right)^{0.5} (\rho_l^{-0.25} + \rho_v^{-0.25})^{-2} , \tag{14}$$

where

$$C_k = \sqrt{3.2} th(0.5\, Bo^{0.25}) , \tag{15}$$

where the Bond number is

$$Bo = D_{h,v} \left[g(\rho_l - \rho_v)/\sigma \right]^{0.5} . \tag{16}$$

Boiling limit

Heat transfer mode in the evaporator is conductive evaporation if the capillary fins are saturated with liquid. The liquid pressure at the evaporator is equal to the saturation pressure at the temperature of the liquid-vapor interface minus the capillary pressure at the liquid-vapor interface.

As a result, the saturation vapor pressure at the fin base temperature exceeds the liquid pressure at the same point. Since this pressure difference increases with the increase of the radial heat flux at the evaporator, vapor bubbles may be formed in the groove. The formation of the vapor bubbles in the groove is undesirable because they can obstruct the circulation of the liquid and cause overheating. The heat transfer mode is consequently shifted and the heat rate in this operation state is termed the boiling limit. Actually, the boiling limit is a limitation of the radial heat flux. Considering the mechanism mentioned above, Chi derived an expression for the boiling limit as follows[13].

$$Q_b = \frac{A_e\, k_{eff}\, T_v}{h_{fg}\, \rho_v\, t_l} \left(\frac{2\sigma}{R_n} - \Delta p_c \right) , \tag{17}$$

where R_n is the bubble size of nucleate boiling, and k_{eff} the effective thermal conductivity of the saturated fins which is given by

$$k_{eff} = \frac{W\, k_l + \delta\, k_{sl}}{W + \delta} , \tag{18}$$

where k_l is the liquid thermal conductivity, and k_{sl} the combined thermal conductivity of the fin and the thin liquid film at the fin tip which is given by

$$k_{sl} = \frac{k_l\, k_s\, t_l}{0.185\delta\, k_s + t_l\, k_l} , \tag{19}$$

where k_s is the thermal conductivity of the fin material. The bubble size of nucleate boiling, R_n, can be selected to be 1×10^{-7} m[13].

Sonic limit

In some heat pipes, especially those with liquid metal working fluids, the vapor velocity may reach sonic value during startup or steady state operation. This choked operating condition is called sonic limit which can be expressed as[13]

$$Q_s = A_v\, \rho_v\, h_{fg} \sqrt{\frac{R_v\, T_v\, \gamma}{2(\gamma + 1)}} , \tag{20}$$

where T_v is the vapor temperature, R_v the gas constant of vapor and γ the ratio of specific heats.

Heating areas in the heat pipe evaporator are arranged for calculation of the performance

8

limitations. Figure 2.4 shows three different heating modes indicated by active film chip resistors. Each chip resistor has a contact heating area of 6.17×12.55 mm², and the shorter side is marked in black as shown in Figure 2.4. Mode 1 heater has only one active chip resistor at the bottom. Mode 2 heater consists of two active chip resistors in the middle. In mode 3 heater, all six chip resistors are switched on. Dimensions of the capillary fin heat pipe used for the calculation are listed as follows:

Total MHP length	108 mm
Inner cross section	10.26×3.91 mm²
L_e(6 chips)/L_a/L_c	18.5/50.6/32.5 mm
Fin length/height/thickness	101.6/0.89/0.1 mm
Fin pitch	0.305 mm
Fin number (one side)	32

Chip resistor (narrow side)   Thermocouple
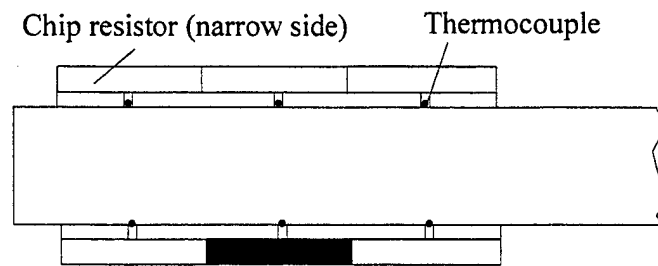
Mode 1
One chip resistor at the bottom is on.
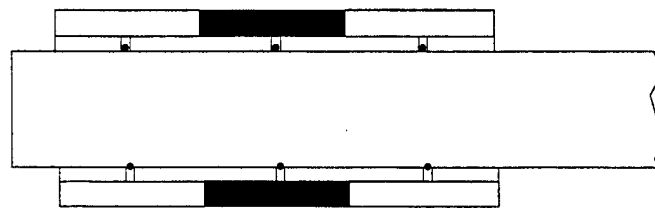
Mode 2
Two middle chip resistors are on.
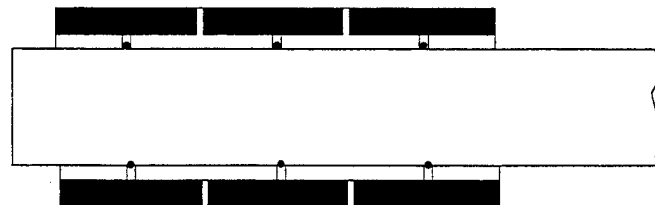
Mode 3
All six chip resistors are on.

Figure 2.4 Evaporator heating modes (referring to Figure 3.7 for a 3-D view).

Using Equations (13), (14), (17) and (20), the performance limitations in relation with the operating temperature are obtained. Profiles of the capillary limit, entrainment limit and boiling limit for the different heating modes, mode 1, mode 2 and mode 3, are presented in Figure 2.5, 2.6 and 2.7 respectively. Meanwhile, these three performance limitations are expressed as evaporator heat fluxes as indicated in Figure 2.5, 2.6 and 2.7. Since the result of the sonic limit is very high compared to the other limits in the temperature range from 10°C to 160°C, the result of the sonic limit is not shown in these figures.

It's indicated that the capillary limit and entrainment limit increase with the operating temperature. The boiling limit decreases with the operating temperature. For mode 1 heater, the capillary limit, entrainment limit and boiling limit are respectively dominant in the temperature ranges of $T_v < 88°C$, $88°C < T_v < 90°C$ and $T_v > 90°C$; for mode 2 heater, they are respectively dominant at $T_v < 54°C$, $54°C < T_v < 105°C$ and $T_v > 105°C$; for mode 3 heater, they are respectively dominant at $T_v < 49C$, $49°C < T_v < 133°C$ and $T_v > 133°C$. The maximum heat rates are 329 W at 90°C for mode 1 heater, 395 W at 105°C for mode 2 heater, and 524 W at 133°C for mode 3 heater.
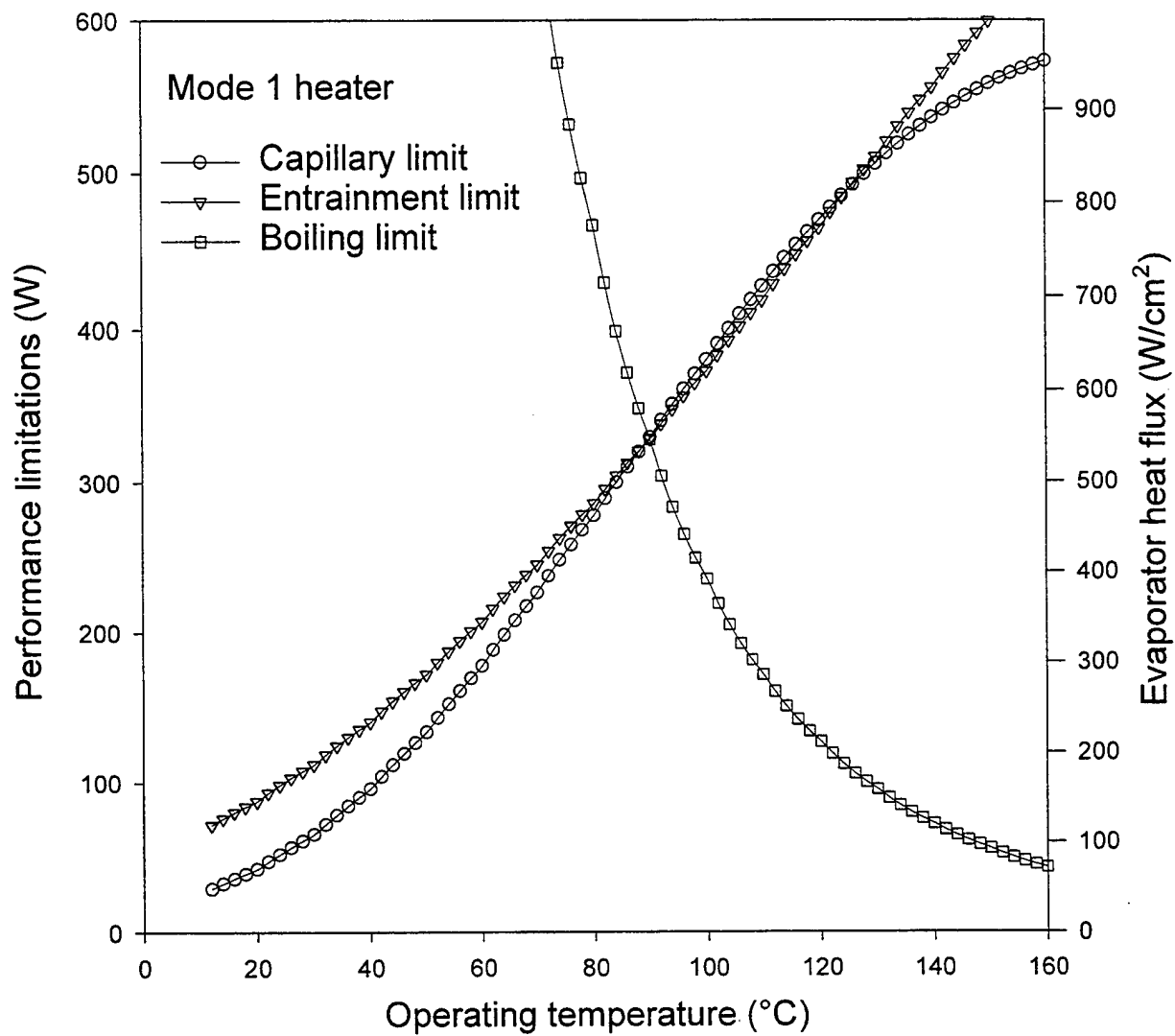
Figure 2.5 Performance limitations of the heat pipe with capillary fins for mode 1 heater.
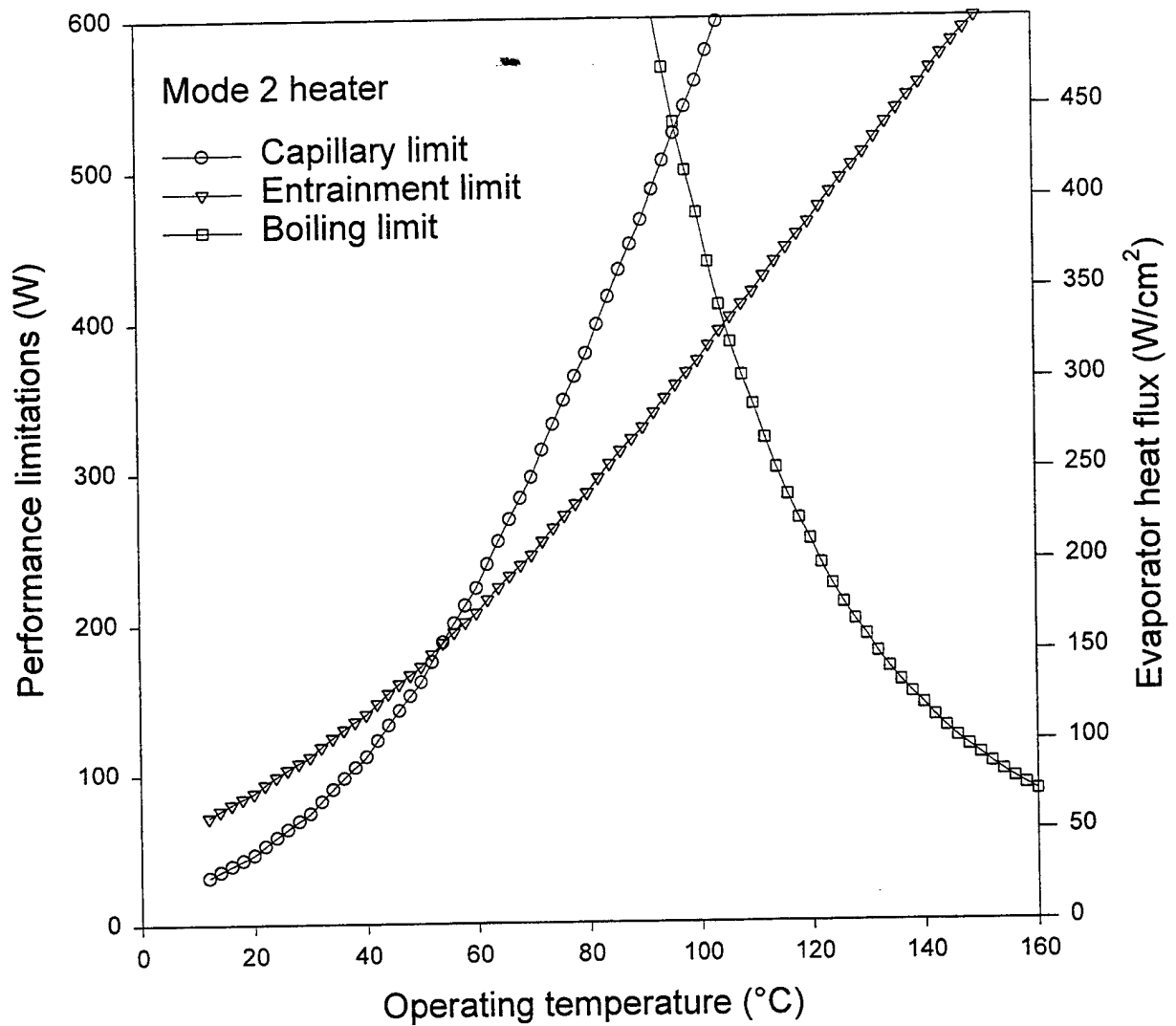
Figure 2.6 Performance limitations of the heat pipe with capillary fins for mode 2 heater.
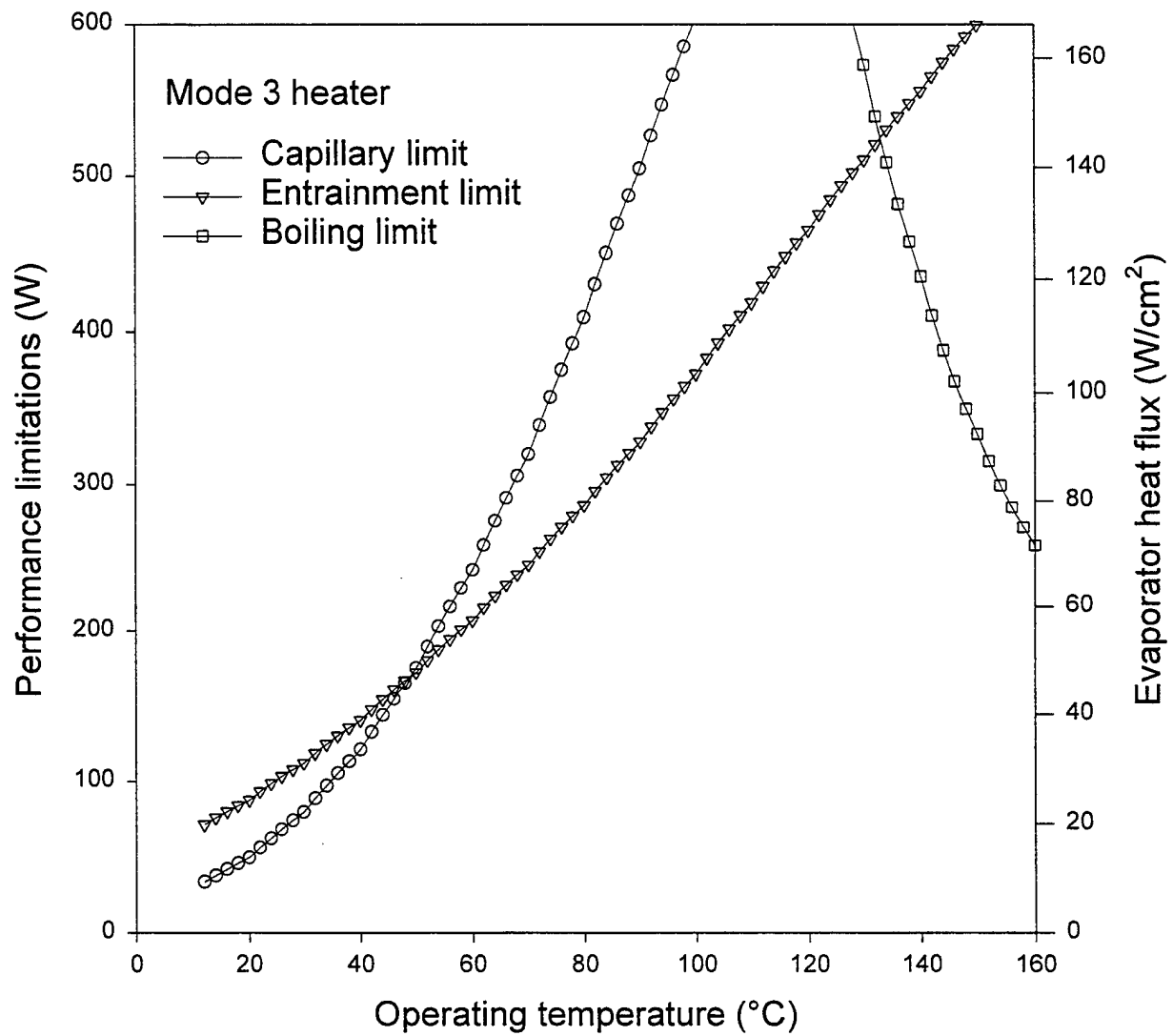
Figure 2.7 Performance limitations of the heat pipe with capillary fins for mode 3 heater.

2.2 Effect of Capillary Structures on Performance Limitations and Thermal Performance Enhancement

In order to achieve maximum heat transport through the heat pipe, trade-off studies between different types of capillary structures and different parameters of geometry should be made. To enhance the capillary pressure, characteristic lengths of capillary structures, e.g., an effective pore radius or a groove width, must be small. However, to decrease the liquid pressure drop in the wick, the pore radius and groove width must be large. In most cases, the heat flux travels radially through the capillary structure to evaporate the working fluid. For a small radial temperature drop through the capillary structure, the capillary structure must be thin and have a high thermal conductivity. This consideration usually requires that the porosity of the capillary structure must be low, which conflicts with the need for a small liquid pressure drop from the condenser to the evaporator. The design of the capillary structure involves a number of factors.

For the axially grooved heat pipe, its performance could be improved by decreasing the groove width and pitch and increasing the groove depth to some extent. This approach is more effective at low operating temperatures, e.g., less than 100°C for the water heat pipe. Considering a constraint of machining cost, a 0.13 mm wide by 0.64 mm deep groove is probably the narrowest and deepest dimension that can be made in aluminum.[14] To reduce the ratio of the groove width to groove depth further, the heat pipe with the capillary fins made by EDM cut is developed by AFRL engineers. Since it is easy to make a very small groove width between two consecutive fins of a folded sheet, a high pumping ability of the capillary fin is achievable at low fabrication cost.

To simplify the fabrication process of the heat pipe, a folded screen is used as the capillary wick[9] as shown in Figure 2.2. The performance limitation of the heat pipe with a folded screen involves also the capillary limit, entrainment limit, and boiling limit. The folded screen with 150×150 mesh has a thickness of 0.11mm and 32 channels on either top and bottom inner walls. The width and height of a closed channel of the folded screen are approximately the same as those of the opened groove between two fins. A hydraulic diameter of the closed channel of the folded screen is a little bit smaller than that of the opened groove between two fins. Consequently, the wick permeability of the folded screen is slightly smaller than that of the capillary fin. To compare the

capillary pumping head of the folded screen with that of the capillary fin, a contact angle between a solid-liquid interface and a liquid-vapor interface for the capillary fin is introduced as shown in Figure 2.8. The contact
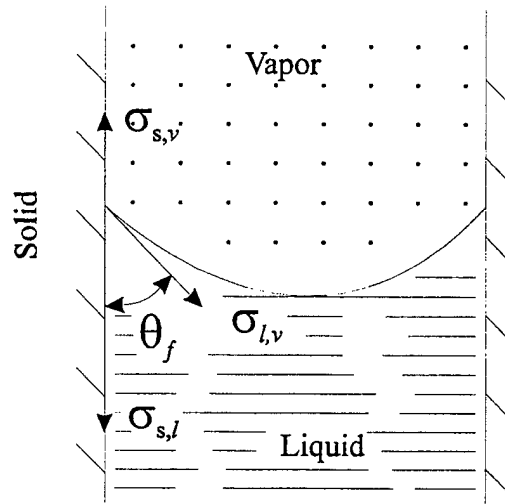
Figure 2.8 Contact angle between a solid-liquid interface and a liquid-vapor interface.

angle, θ_f, is given by the following Young's equation.[4]

$$\theta_f = \cos^{-1}\left(\frac{\sigma_{s,v} - \sigma_{s,l}}{\sigma_{l,v}}\right), \tag{21}$$

where $\sigma_{s,v}$, $\sigma_{l,v}$ and $\sigma_{s,l}$ are the surface tensions of the solid-vapor, liquid-vapor and solid-liquid interfaces. For water, $\sigma_{s,v} > \sigma_{s,l}$ and the contact angle is acute. For the folded screen, the screen wick is filled with water and the contact angle is given by

$$\theta_w = \cos^{-1}\left(\frac{\sigma_{w,v} - \sigma_{s,l}}{\sigma_{l,v}}\right), \tag{22}$$

where $\sigma_{w,v}$ is the surface tension at the interface between the saturated screen wick and vapor. In the case of the copper screen saturated with water, $\sigma_{w,v} < \sigma_{s,v}$. As a result, the contact angle for the folded screen, θ_w, is greater than that for the capillary fin, θ_f. According to eqn. (12), the greater the contact angle, the smaller is the pumping head. Hence, the pumping head of the folded screen is smaller than

16

that of the capillary fin. Moreover, the permeability of the folded screen is not greater than that of the capillary fin. It is therefore concluded that the capillary limit is smaller for the folded screen than for the capillary fin. The calculation of the entrainment limit for the folded screen can be based on the same formula and geometric parameters as for the capillary fin. As a result, the entrainment limit for the folded screen is approximately the same as for the capillary fin. Since there is an additional thermal contact resistance between the screen wick and the heat pipe wall and the effective thermal conductivity of the saturated screen wick is smaller than that of the capillary fin, the boiling limit is smaller for the folded screen than for the capillary fin though the correlation of the boiling limit for the folded screen is not available.

In order to enhance the maximum performance and thermal performance of the heat pipe, a high performance MHP is developed that consists of two folded copper sheet fins with notches cut at the top of the fins in the evaporator and condenser. Each fin is brazed onto either wide side of the MHP. Figure 2.9 shows the folded sheet fins with notches cut at the top of the fins in the evaporator and condenser. The fin bridges (uncut part) separating notches on the top of the fins protect a return liquid against the interfacial shear stress of countercurrent two-phase flow to some extent. Meanwhile, the cut holes let the vapor escape from the groove into the vapor core. The uncut part of the folded fin in the heat pipe condenser serves as additional secondary heat transfer area and contributes to the enhancement of condensation heat transfer.

The present experimental investigation is focused on the thermal performance of above mentioned capillary structures at high heat fluxes in the evaporator. Some modifications of these capillary structures will be made to cover more capillary structures for the test.
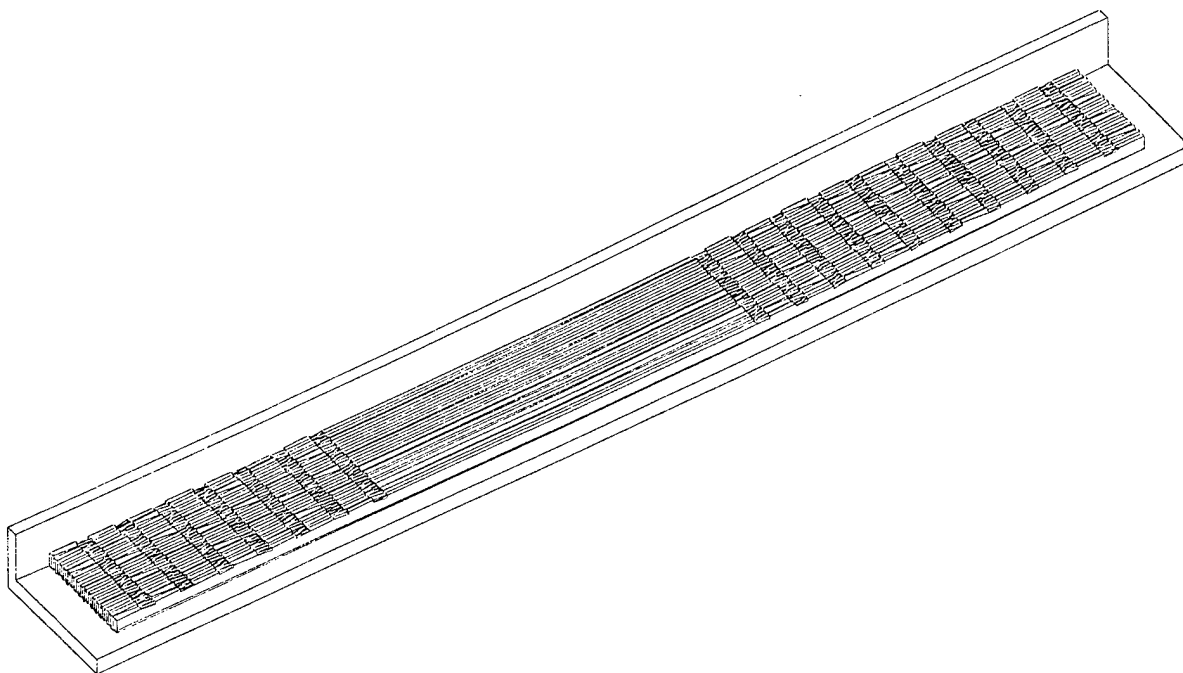
Figure 2.9 Folded sheet fins with notches cut at the top of the fins in the evaporator and condenser.

3   EXPERIMENTAL INVESTIGATION OF MINIATURE HEAT PIPES

3.1   Design and Fabrication of Miniature Heat Pipes for Test

New capillary structures are fabricated for high performance MHPs. The capillary structures rely on the use of a folded copper sheet fin (group I) and a folded copper screen (group II) which are available from Robinson Fin Machines, Inc. The description of MHP test hardware is presented in Table 3.1.

Table 3.1 Description of MHP test hardware

Group	Name	Capillary wick configurations (copper)	Container & end caps	Fill (ml)	Remarks
I	A	Folded sheet fin (FSF) without cut	All brazed	1.4 0.89	16 open & 16 closed channels on each top & bottom
	B	FSF with full cut on the top	All brazed	1.3 0.87	32 open channels on each top & bottom
	C	FSF with top cuts in evaporator & condenser	All brazed	0.87	1" top cuts Damaged during assembling heaters
	D	FSF with notches cut in evaporator & condenser	All brazed	1.3 0.85	1.27 mm wide cuts at 3.81 mm interval
II	E	Folded screens separately Brazed on top & bottom	All brazed	1.1	32 channels on each top & bottom, no wick on two sides
	F	Folded screen	End caps welded	1.0	Mechanically inserted wick without stiffener, 82 total channels with 32 channels on each top & bottom
	G	Folded screen with two stiffeners	End caps welded	0.69 1.0 1.1	Mechanically inserted wick with stiffeners, 82 total channels with 32 channels on each top & bottom

The type of the folded sheet fin (FSF) can be extended to three different fin shapes with different cutting patterns or without any cutting on the fin top, which are related with heat pipe A, B and D as described in Table 3.1. The fin shape for heat pipe A is formed with a folded copper sheet brazed on each wide side of the heat pipe. On the outer wall of the wide side, the film chip resistors are mounted for heat generation as shown in Figure 2.4. Heat pipe B contains the capillary fins that are fabricated by brazing the folded sheet on the wide side wall and making a full cut at the top of the fins. The EDM technology is applied to the cutting process. Heat pipe D involves the folded sheet fins with notches cut at the top of the fins in the evaporator and condenser. Cutting notches at the top of the fins in the evaporator and condenser, instead of making a full cut, will reduce the average counter-current flow shear stress acting on the liquid-vapor interface in the heat pipe. The notch cuts enable the vapor to release from the partially covered grooves into the vapor core. The schematics of heat pipes A, B and D are shown in Figure 3.1.

The dimensions of the capillary fin assembly for heat pipe B are shown in Figure 3.2. The full cut is made throughout the top of the fins. For heat pipe D, the similar folded sheet is used but notch cuts at the top of the fins are made instead of the full cut. The dimensions of the folded sheet fins with notch cuts are shown in Figure 3.3. The notch cuts are evenly distributed along the heat pipe length and made only in the evaporator and condenser sections. The geometric parameters of the fin assemblies for heat pipe B and D are included in Table 3.2. Two similar assemblies are required to build a heat pipe. In Table 3.2, the inner cross section refers to the cross-sectional area bounded by the inner wall and the outer cross section to the heat pipe outer wall. The evaporator length is related with mode 3 heater as shown in Figure 2.4. The notch pitch is set along the heat pipe length. The brazing temperature for the assembly of the heat pipe parts is 655°C. Figure 3.4 shows all parts for the assembly of heat pipe B. These parts include two copper angles holding the capillary fins, two end caps, and one copper tube for the filling of working fluid. The brazing material is used at the junctions of the parts. Figure 3.5 shows a photographic view of heat pipe D parts.
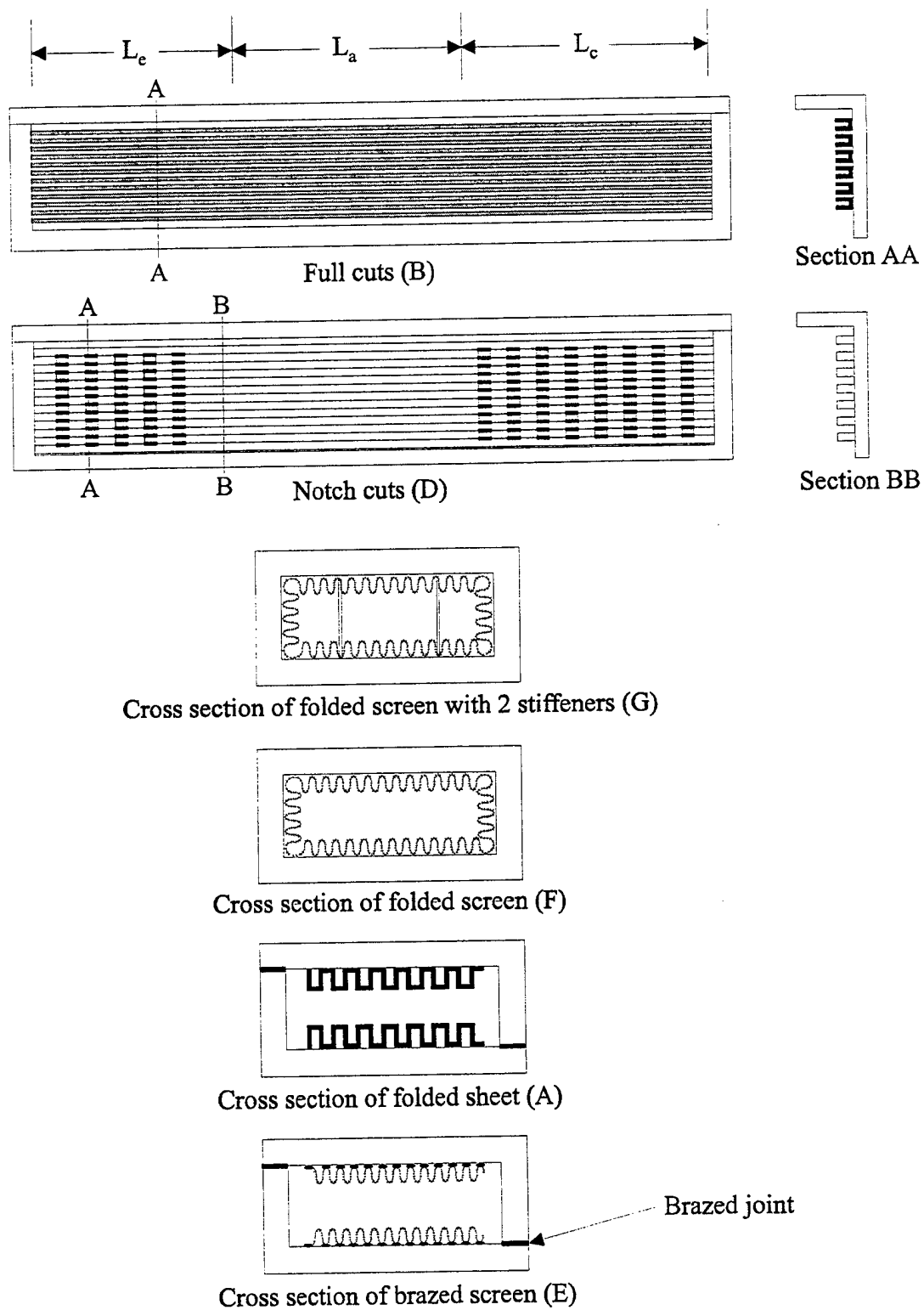
Figure 3.1 Schematics of MHPs.

Table 3.2 Geometric parameters of the fin assemblies for heat pipe B and D.

Parameters	Heat pipe B	Heat pipe D
Total MHP length	108 mm	108 mm
Inner/outer cross section	10.26×3.91/12.7×6.35 mm^2	10.26×3.91/12.7×6.35 mm^2
L_e(6 chips)/L_a/L_c	18.5/50.6/32.5 mm	18.5/50.6/32.5 mm
Notch number	Full cut	7(in evaporator)/10(in condenser)
Fin length	101.6 mm	101.6 mm
Fin height	0.89 mm	1.02(uncut)/0.89(cut) mm
Fin thickness	0.1 mm	0.1 mm
Fin pitch	0.305 mm	0.305 mm
Fin number (one side)	32	32
Notch cut width/depth	-	1.27/0.13 mm
Notch cut pitch	-	3.81 mm
Angle wall thickness	1.22 mm	1.22 mm
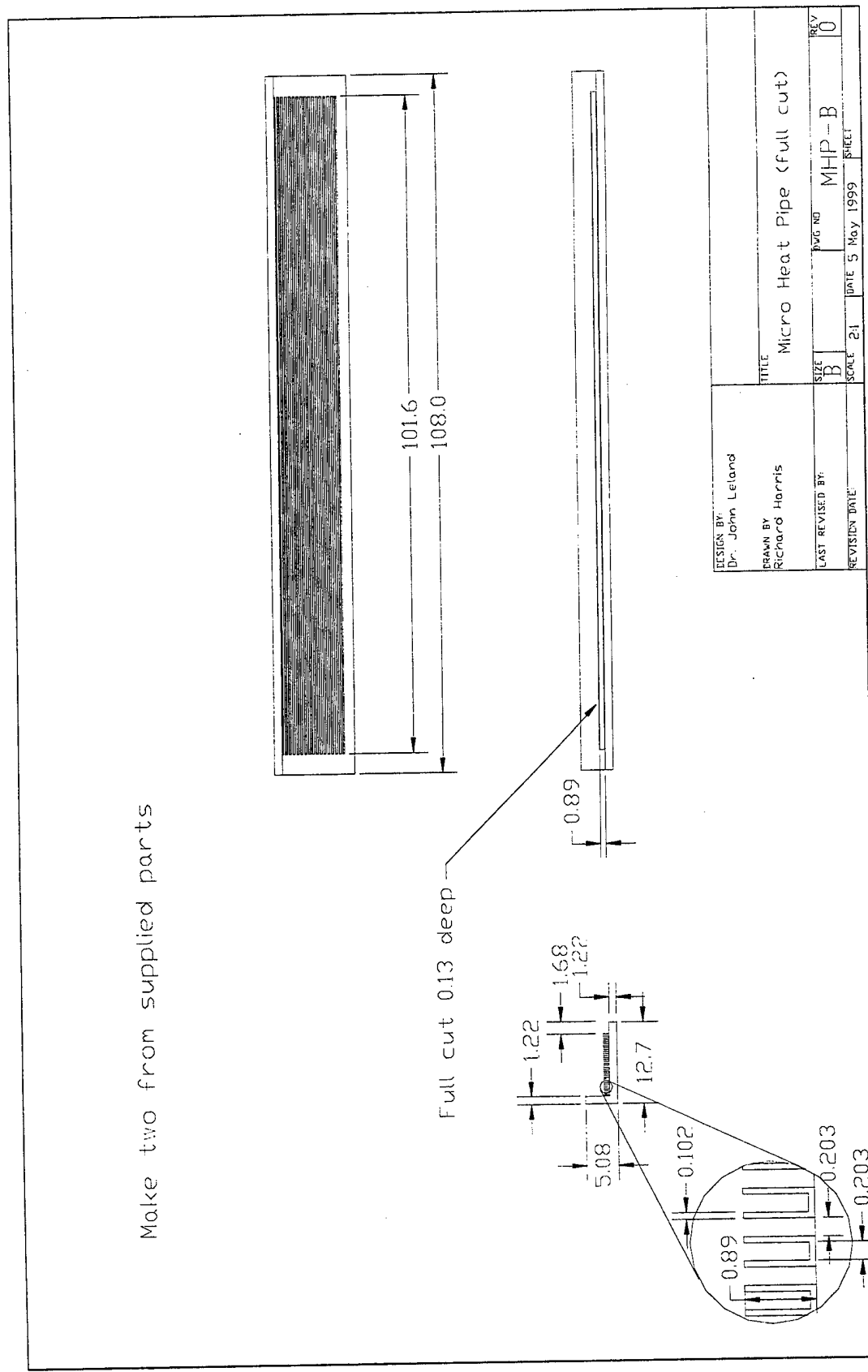
Figure 3.2 Dimensions of capillary fin assembly (dimensions in mm).
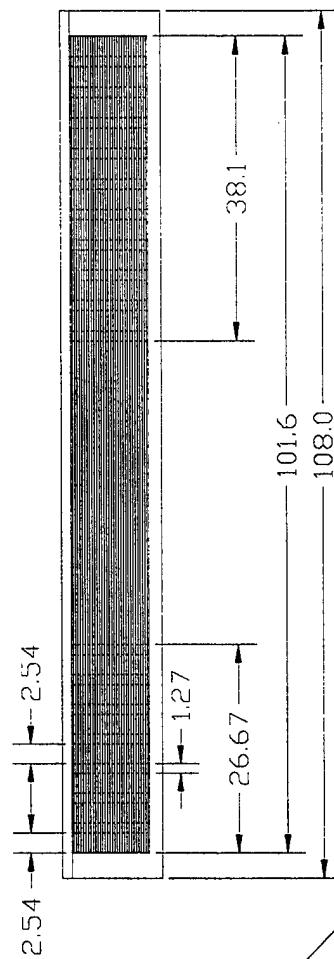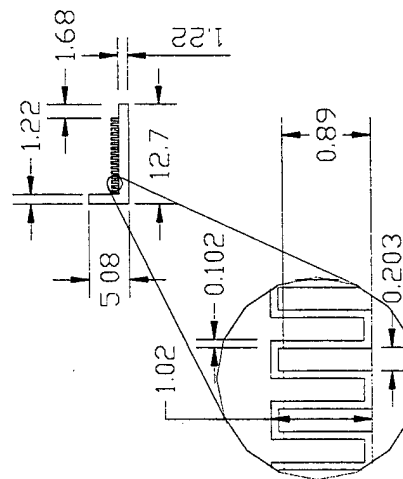
Figure 3.3 Dimensions of folded sheet fins with notch cuts in the evaporator and condenser (dimensions in mm).
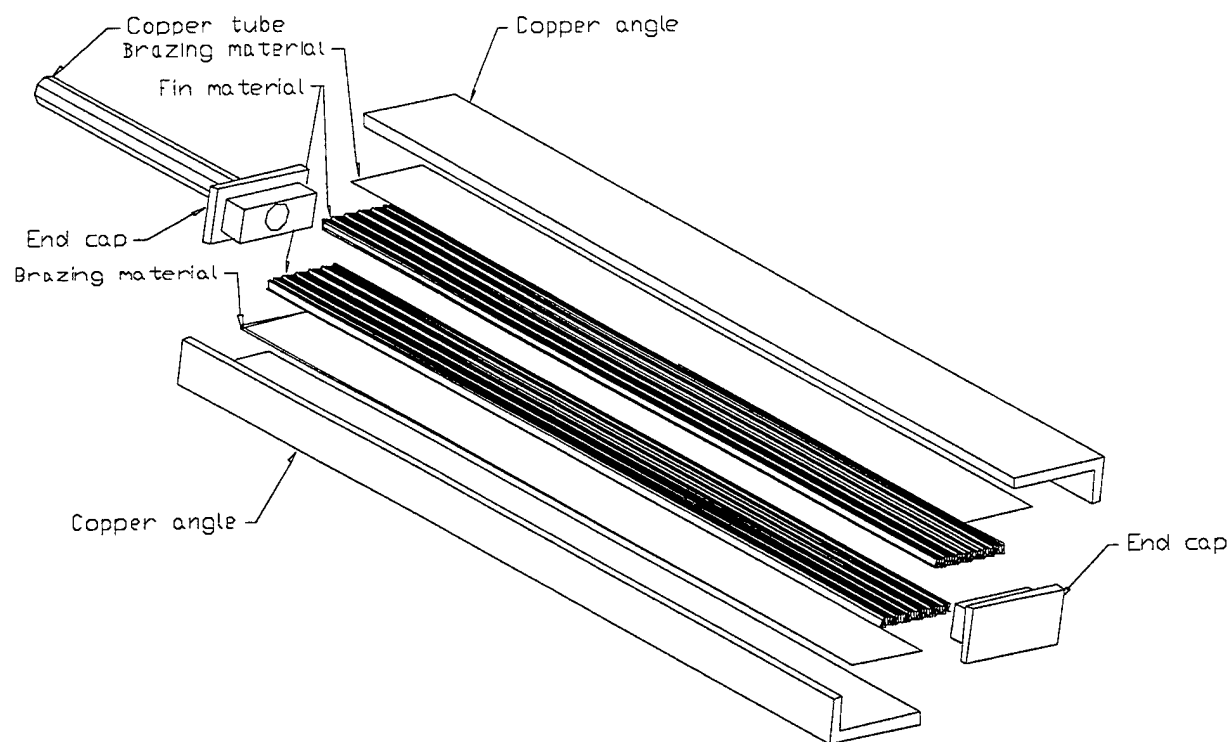
Figure 3.4   Assembly of the heat pipe B with capillary fins.
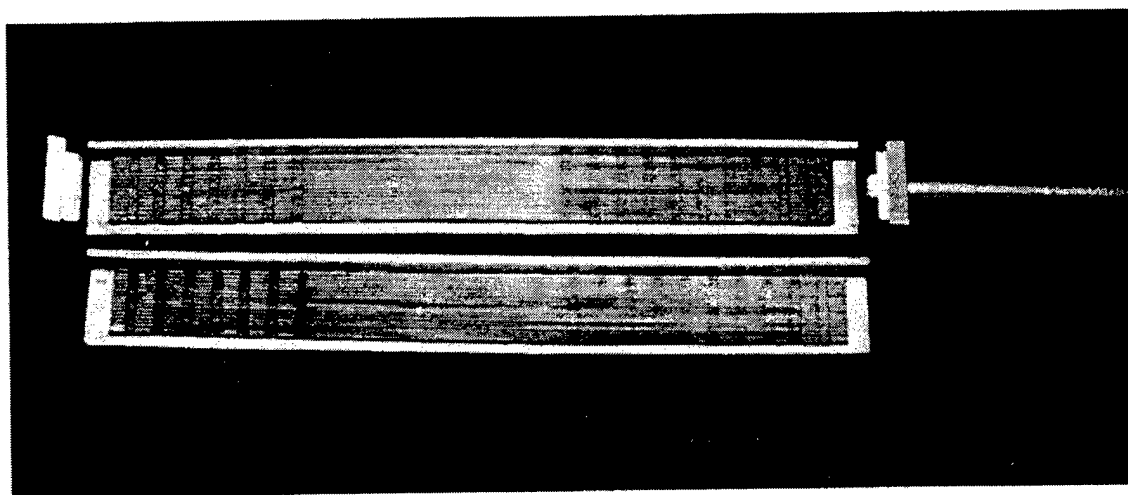
Figure 3.5   Photographic view of heat pipe D parts.

The type of the folded screen involves two different screen mounting processes such as brazing the folded screen onto the wide side of heat pipe and wrapping the folded screen around the inner wall. The former is related with heat pipe E and the latter with heat pipe F and G, as depicted in Table 1. The difference between heat pipe F and G is that heat pipe G has two stiffeners holding the folded screen against the heat pipe wall and heat pipe F does not have any stiffener. The use of the stiffener enhances the thermal contact conductance between the folded screen and the heat pipe wall. Schematic cross-sectional views of heat pipe E, F and G are shown in Figure 3.1. The folded screen channel width for heat pipe E, F and G is approximately the same as the groove width between two fins for heat pipe A, B and D. The folded screen has 150x150 mesh that is inserted into the heat pipe. The thickness of the copper screen is 0.11 mm and the length (in axial direction) is 102 mm. The folded screen used in heat pipe E has a width of 9.75 mm (on the heat pipe cross section) covering 32 folded grooves. The copper angle on which the folded screen is brazed has the same dimension as used for the fin heat pipes (A, B and D). The cross-sectional dimensions of heat pipe G are shown in Figure 3.6. Heat pipe F has the same dimensions of the folded screen and container
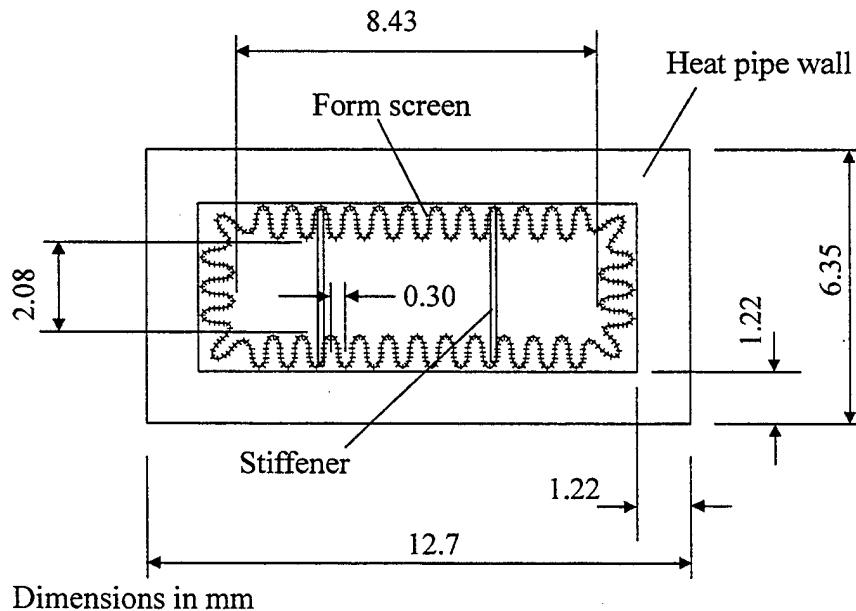
Figure 3.6 Dimensions of heat pipe G with a folded screen and two stiffeners.

wall as heat pipe G. The heat pipe container dimensions for the folded screen heat pipes are the same as the case of the fin heat pipes (A, B and D). In the case of heat pipe F and G, the heat pipe container is made of a rectangular tube, and the two end caps are welded with the container during assembly. The assembly of heat pipes F and G is the simplest of all present MHPs.

The heat pipes are baked at 150°C, evacuated to a pressure of 3×10^{-6} Torr for 24 hours, and filled with distilled water. After the filling, the copper tube is pinched and welded. The fill amounts measured at 25°C for every MHP are also given in Table 3.1. The fill amount is varied to find the desired value for the superior thermal performance. A ratio of the working fluid fill amount to the volume of all the grooves is an important parameter and is referred to as fill ratio. The 0.87 ml fill amount for heat pipe B corresponds to a fill ratio of 80%; the 0.85 ml fill amount for heat pipe D corresponds to a fill ratio of 78%; the 1.1 ml fill amount for heat pipe G corresponds to a fill ratio of 72%. Table 3.1 also briefly shows the assembly methods for each heat pipe. It should be pointed out that using those capillary wick structures presented in Table 3.1 makes it possible to fabricate narrow and deep capillary grooves as desired from the point of view of enhancing capillary limit of the heat pipe.

3.2 Experimental Set-up and Procedure

Figure 3.7 shows a typical heat pipe assembly used for the performance test and gives overall dimensions along the heat pipe length. Six thick film resistors are used to simulate the heat source of electronic components, three on the top and three on the bottom of the heat pipe. Thermocouple locations on the heat pipe are shown in Figure 3.8. There are eight thermocouples at the top surface, and eight at the bottom surface in the symmetric positions in reference to the thermocouples above. Three thermocouples are placed on the side-wall of the MHP. Two intermediate plates with three slots are soldered onto the evaporator and another two plates with two slots are soldered onto the condenser to protect the thermocouples against a contact with the heater or cooler. Six thermocouples in the evaporator and four thermocouples in the condenser are inserted into the thermocouple slots and soldered onto the heat pipe wall. The slot width is 0.51 mm and is sized to accommodate the thermocouple wire of 0.08 mm in diameter and 0.3 mm in bead diameter. Epoxy is filled in the thermocouple slots to insulate the thermocouple from the chip heater and from the cooler. The film resistors are soldered onto the top and bottom intermediate plates in the evaporator, making the intermediate plate sandwiched between the chip resistor and the heat pipe. Figure 3.9 shows a photographic view of the heat pipe D assembly with thermocouple wires.
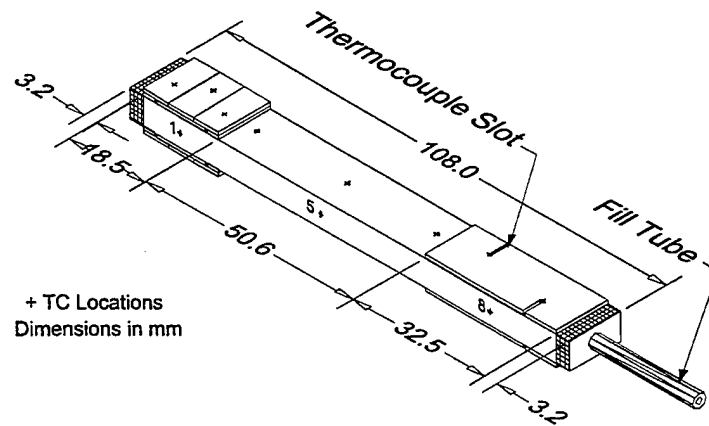
Figure 3.7   Axial dimensions of MHPs.

Heat pipe end (excluding cap)
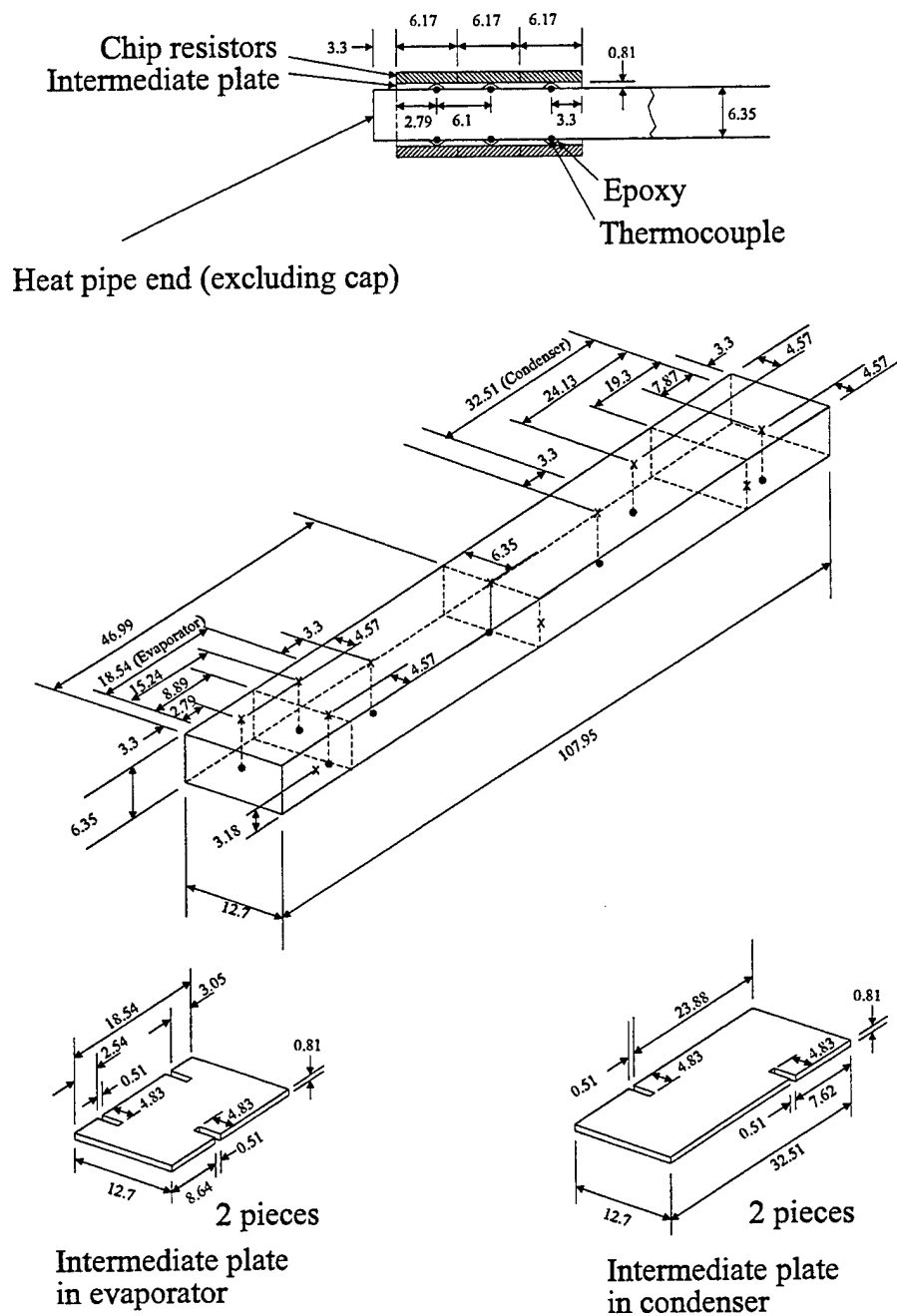
3-D drawing of thermocouple locations on MHP
x Visible thermocouple
• Hidden thermocouple

Figure 3.8   Thermocouple locations (19 thermocouples, type T)
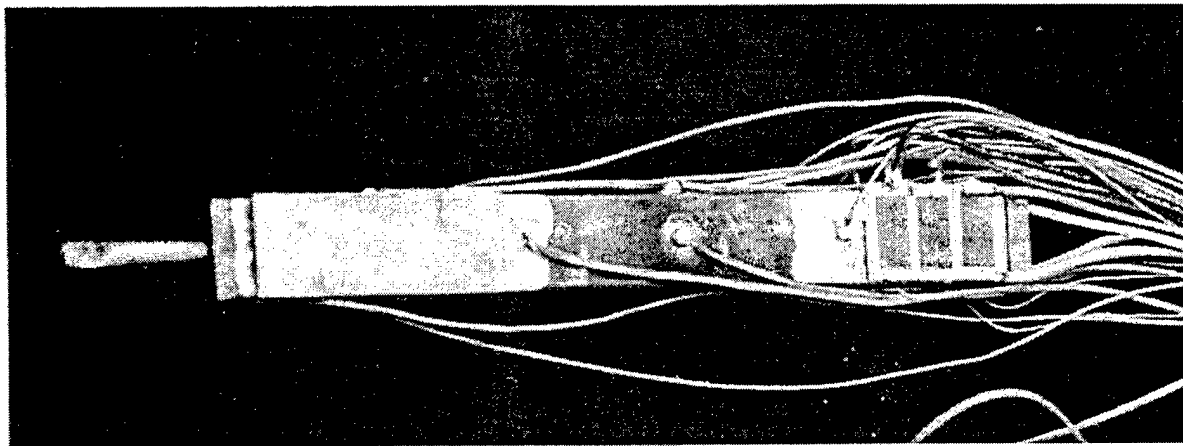
Figure 3.9 Photographic view of the heat pipe assembly with thermocouple wires.

The schematic of a MHP experimental setup is shown in Figure 3.10. A photographic view of the experimental setup is shown in Figure 3.11. A DC power supply unit is used to provide DC power for the heaters. The chip resistors are built in parallel and connected with switches so that the chip resistors can selectively be turned on and off to arrange different heating modes. Two copper coolers are clamped onto the top and bottom intermediate plates of the heat pipe condenser.

. Inside the cooler, there is a rectangular channel with plain fins mounted on its contact side with the condenser. Two turbine flow meters are used to measure the coolant flow rates through the top and bottom coolers. The turbine flow meter is operated with a signal conditioner. The coolant flow rates are regulated by two valves in the upper and lower flow channels. The flow rates through the top and bottom coolers are set to be approximately equal. The coolant temperatures at the inlet and outlet of the coolers are measured using two type T probe thermocouples. The coolant temperature is regulated by a constant temperature bath (cold bath) with 500 W capacity. A pressure transducer is installed at the coolant channel to measure the coolant supply pressure that is partially controlled by a bypass valve. The coolant flow circulation is maintained by a water pump.

The experimental investigation focuses on the heat transfer characteristics of the MHPs with different fill amounts of the working fluid (water) at various heat rates and operating temperatures. The operating temperature, T_v, is indicated by the thermocouple in the middle of the adiabatic section. The operating temperature is adjusted by regulating the coolant flow rate and the cold bath temperature. The experimental parameters are listed as follows:

30
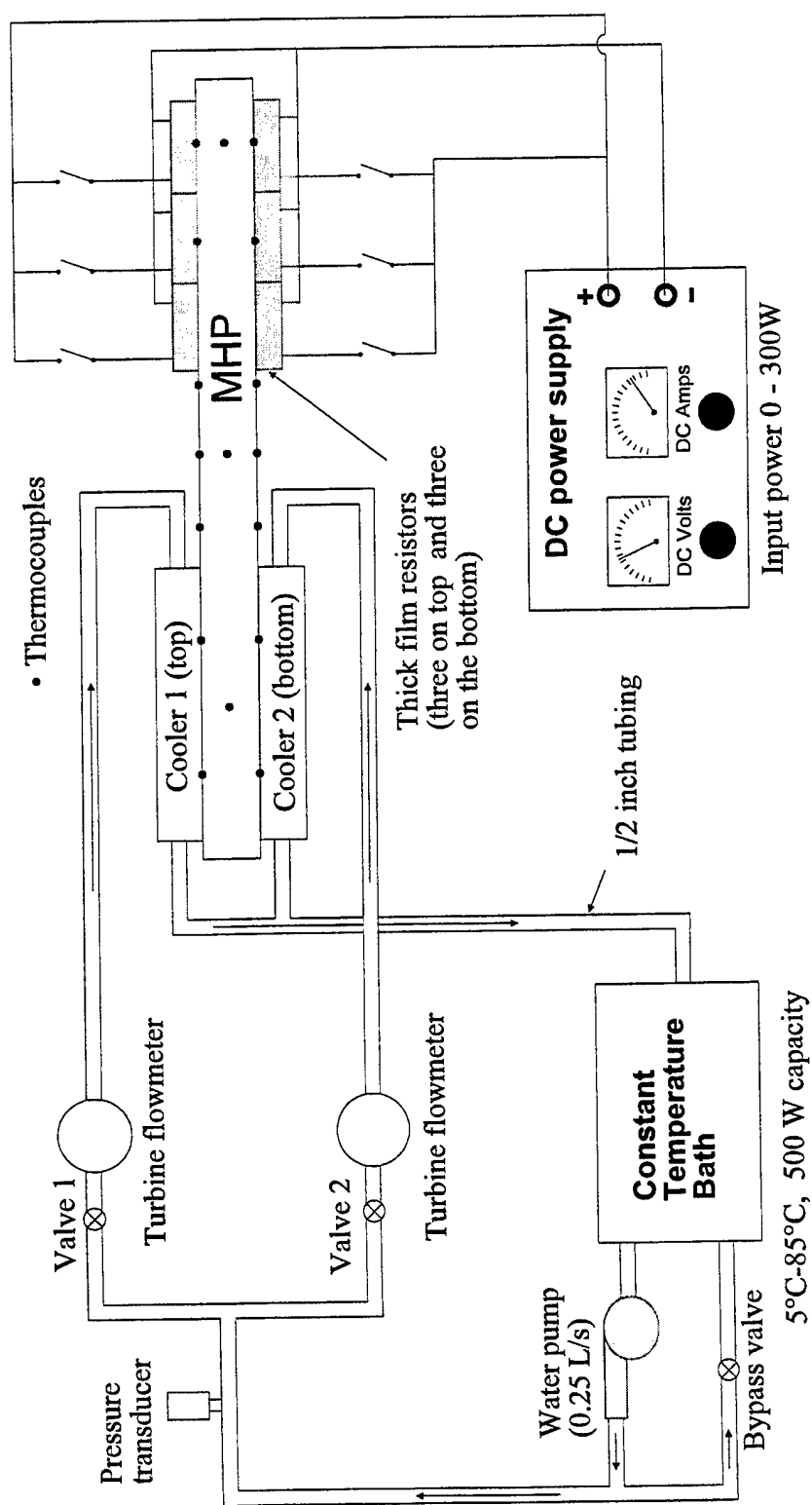
Figure 3.10   Schematic of MHP setup

31
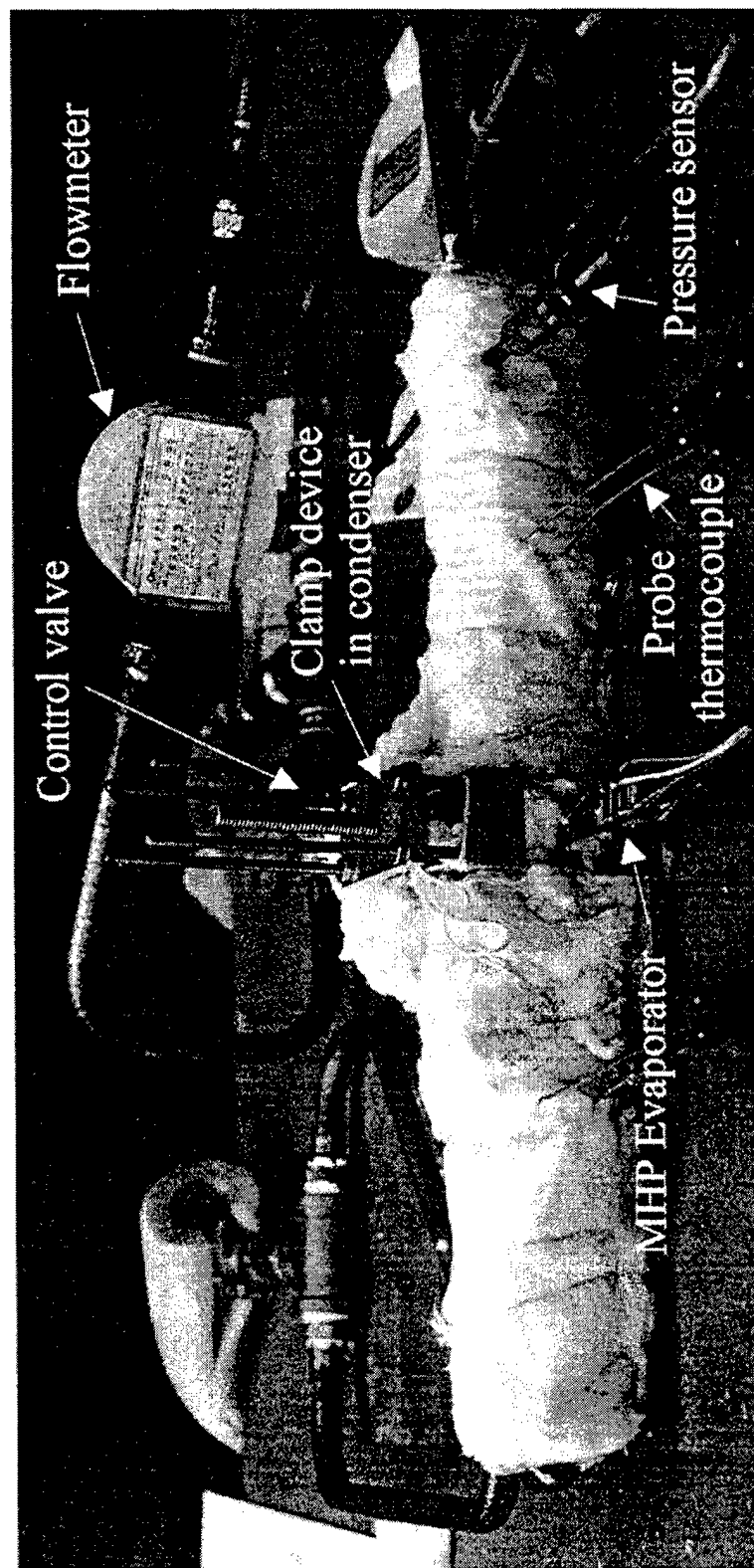
Figure 3.11 Photographic view of the MHP setup.

32

Operating temperature:	60°C, 80°C, 90°C, 100°C, 110°C.
Input power:	Greater than 10W.
MHP orientation:	Horizontal operation.

The active film chip resistors are arranged in the following different modes accounting for different heating areas as shown in Figure 2.4.

Mode 1: 1 chip on the middle bottom.

Mode 2: 1 chip on the middle top and 1 on the middle bottom.

Mode 3: 3 chips on the top and 3 on the bottom.

Each chip resistor has a contact area of 6.17×12.55 mm^2 with the heat pipe.

The actual total heat rate through the heat pipe is estimated by subtracting heat losses, Q_{loss}, from the input power. To measure the heat loss at various specific heat pipe operating temperatures, a small electric power load is applied to the chip resistor on the heat pipe with coolers removed. The whole heat pipe is insulated. The value of the applied electric power load is adjusted until a specific operating temperature is reached. As a result, the heat losses of 1.2 W, 2.15 W and 2.90 W were measured at the operating temperatures of 60°C, 90°C and 110°C. With the tested heat losses at various operating temperatures, the actual total heat rate is obtained as follows

$$Q = IV - Q_{loss},\tag{23}$$

where I is the total electric current through the heaters on the heat pipe and V is the voltage across the heaters.

For heat transfer analysis, average temperatures in the evaporator, condenser and adiabatic section are calculated. The average evaporator temperature is an arithmetic average on temperatures indicated by the thermocouples covered with the active chip resistors. For mode 1, mode 2 and mode 3 heating configurations, the average temperature respectively involves one thermocouple, two thermocouples and six thermocouples. The average adiabatic temperature involves two thermocouples on the middle top and bottom surfaces of the adiabatic section. The average condenser temperature involves four thermocouples on the top and bottom surfaces of the condenser.

3.3 Measurement Uncertainty

The Hewlett Packard 3852A data acquisition system is used to make all temperature measurements. This device has a resolution of 0.02°C and a rated accuracy of 0.65°C for type T thermocouple. The data acquisition unit and type T thermocouples (19 0.08 mm diameter thermocouples and 4 probe type thermocouples) are compared to a precision digital RTD with 0.03°C rated accuracy over the range of interest and the system accuracy is found to be within 0.1°C. In the steady state, the wall thermocouples fluctuate within 0.2°C. The accuracy of the thermocouple locations is within 0.5 mm in the heat pipe axial direction.

The actual total heat rate (Q) through the heat pipe is estimated based on the measurement of heat losses of the insulated heat pipe with coolers removed. The DC power applied to the heat pipe is supplied by the Hewlett Packard 6030A System Power Supply unit. The accuracy of the voltage is 0.035%+145 mV and the accuracy of the current is 0.02%+25 mA. The overall uncertainty of the heat rate through the heat pipe is predicted using the standard Kline and McClintock approach to the calculation of random uncertainty[15]. The same approach is taken for the calculation of other overall uncertainties hereafter. For heat pipe B (HP B) with 0.87 ml fill amount, the predicted overall uncertainty of the heat rate is shown in Figure 3.12. The uncertainty of Q varied from 5.7% at 10 W input power to 0.8% at 210 W input power. The uncertainty of Q for other MHPs varies only slightly compared to the case of HP B.

To compare the heat rate through the top cooler (Q_{top}) and bottom cooler (Q_{bot}) at heat rates higher than 90 W, calorimetry is applied by measuring the flow rate of the coolant and the coolant temperatures at the inlet and outlet of the coolers. Two turbine flow meters (OMEGA FP-541 flow sensor) working with signal conditioners are used to measure the coolant flow rate. The turbine flow meters are calibrated for water. The uncertainty of the turbine flow meter is 0.5% of full scale. The uncertainties of Q_{top} and Q_{bot} are predicted for various operating conditions. Typically, the results for HP B are also shown in Figure 3.12. The results are associated with mode 2 and mode 3 heaters and with the operating temperatures of 60°C to 110°C. It is indicated that the uncertainties of Q_{top} and Q_{bot} decrease with an increase in the input power and range between 14% and 26% at the input power of 90 W to 210 W. It should be pointed out that the uncertainty of the heat rates could be controlled

34

by setting an appropriate flow rate range. It is also indicated in Figure 3.12 that the uncertainty of the total heat rate predicted by measuring the heat losses is much smaller than that of Q_{top} and Q_{bot} estimated by using the calorimetry. That is the reason why the measurement of heat losses is used as the actual heat rate through the heat pipe.

All of the experimental data such as the temperatures, the input power and the coolant flow rates are acquired 50 times in an interval of 1 minute and the average values on the 50 consecutive data are recorded after a steady state is reached. The use of the mean values is appropriate to reduce the effect of the fluctuation of the tested parameters at high heat fluxes in the evaporator.

Overall uncertainties of the heat transfer coefficients of evaporator and condenser are estimated. For HP B with 0.87 ml fill amount, the predicted overall uncertainties for h_e and h_c are shown in Figure 3.13. The highest uncertainty for h_e and h_c occurs at the lowest input power. Given an input power, the uncertainties h_e and h_c are the highest for mode 1 heater and the lowest for mode 3 heater. This is because a different thermocouple number is used for each heating mode. The uncertainty decreases more noticeably for h_c than for h_e with an increase in the input power. The variation of uncertainties for different MHPs is less than 2% under the same operating conditions.
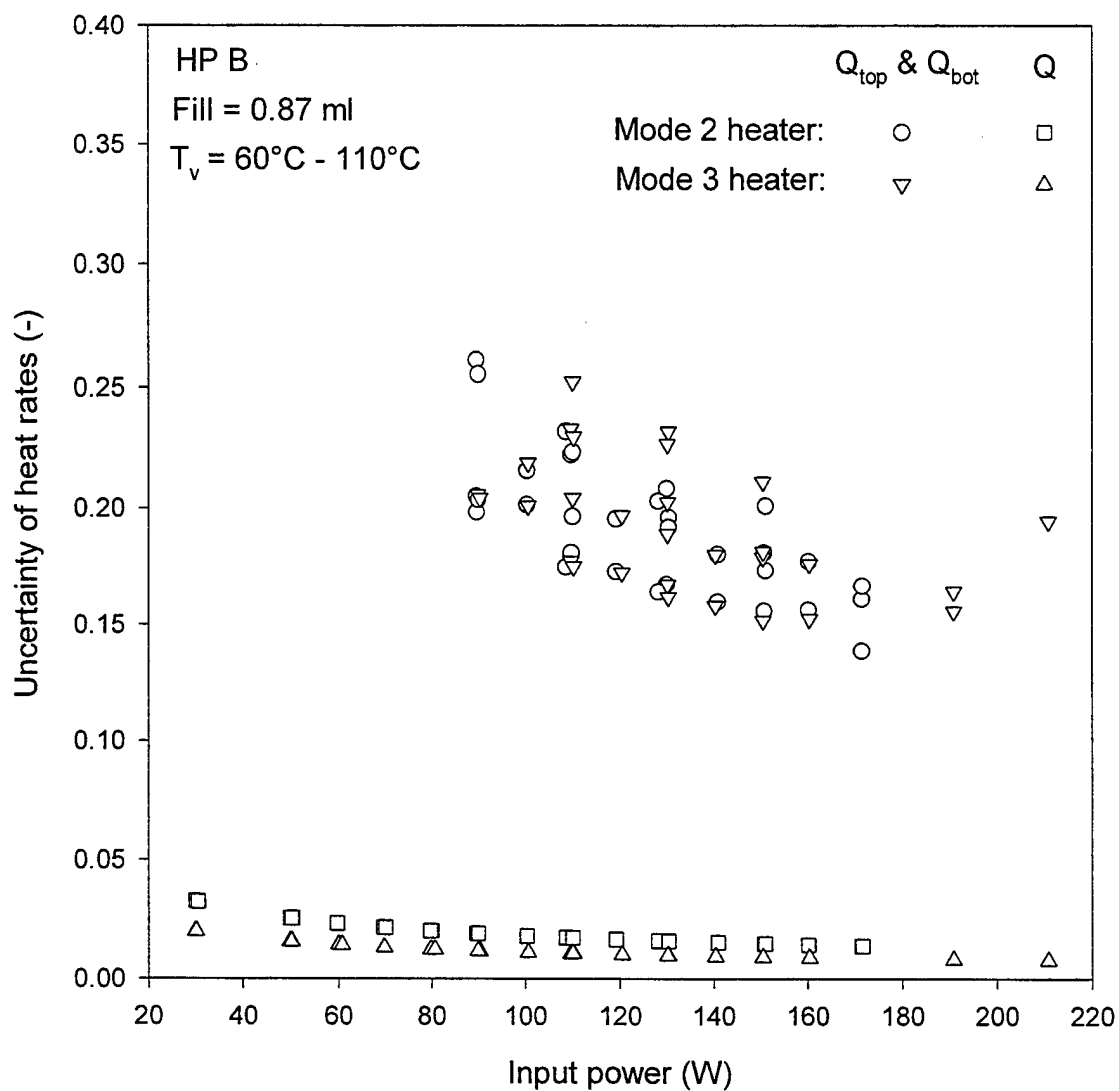
Figure 3.12 Uncertainties of the total heat rate through heat pipe B, the heat rate through the top condenser (Q_{top}) and through the bottom condenser (Q_{bot}) in relation with the input power.
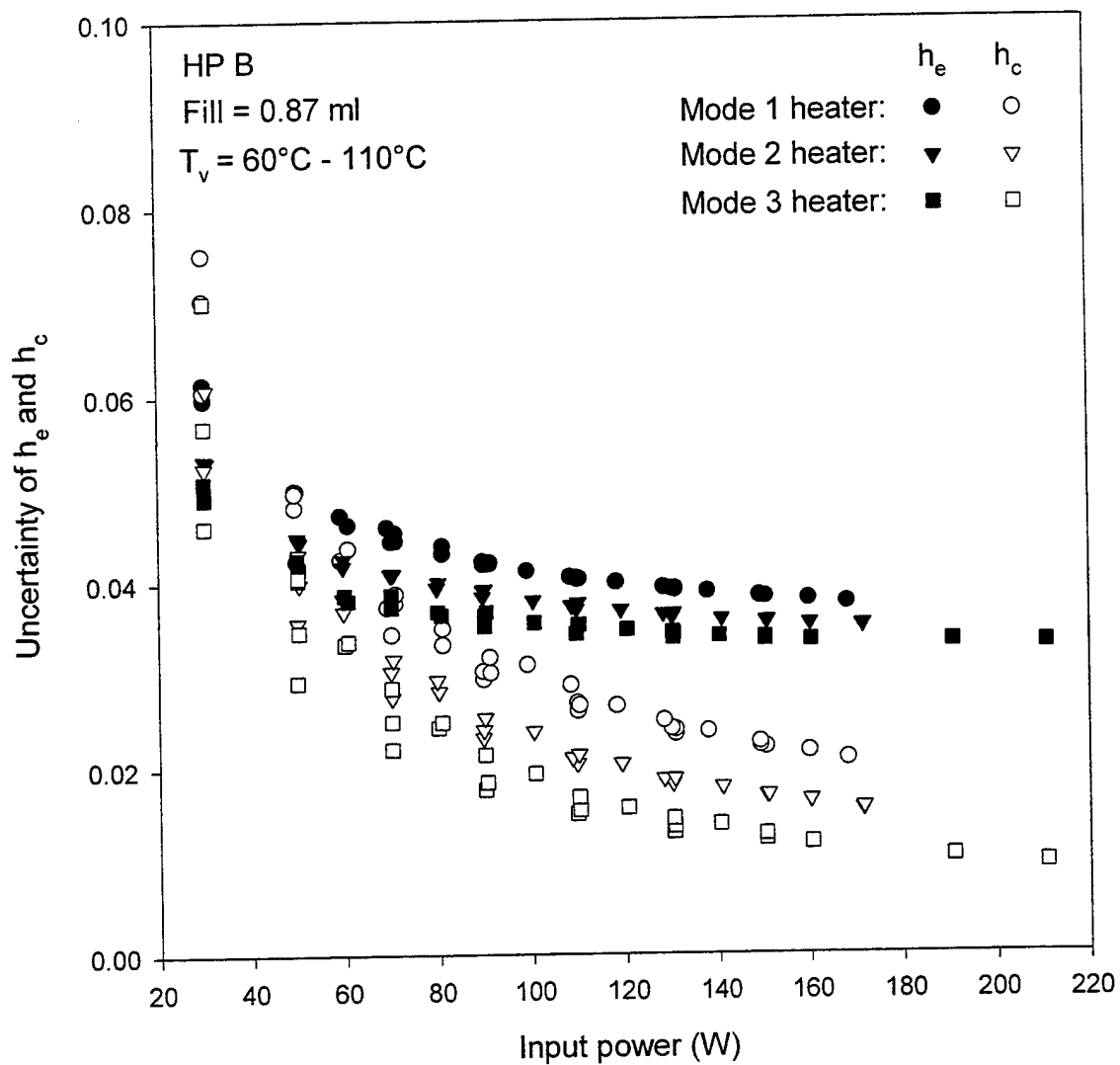
Figure 3.13   Uncertainties of the heat transfer coefficients of evaporator and condenser for heat pipe B in relation with the input power.

3.4 Thermal Performance Results and Discussion

First of all, the experimental investigation on thermal performance of the heat pipes listed in Table 3.1 is conducted to determine appropriate fill amounts for the heat pipes with different types of capillary structures. Primary thermal performance results for the folded screen heat pipe group or the capillary fin heat pipe group are compared and favorable capillary structures are further selected. More experiments are conducted at various operating temperatures and heat rates and results are compared for the heat pipes with the preferable fill amounts and capillary structures. Based on the experimental result of the thermal performance at achievable heat transport rates, the different capillary structures are evaluated.

3.4.1 Preferable capillary structures and fill amounts

In the group of folded screen heat pipes with a fill amount of 1.0 or 1.1 ml, the average evaporator-to-condenser temperature difference, ΔT_{ec} ($\Delta T_{ec} = T_{e,m} - T_{c,m}$), of heat pipe G is the smallest at heat rates greater than 19 W. The ΔT_{ec} for heat pipe E is slightly smaller than that for heat pipe F. For example, with mode 2 heater at a 58 W heat rate and $T_v = 90°C$, the ΔT_{ec} is 25.2°C for heat pipe E, 27.5°C for heat pipe F and 20.5°C for heat pipe G. Brazing the folded screen on the heat pipe wall causes a twofold effect. It reduces a contact thermal resistance at the heat pipe wall. On the other hand, the brazing material may fill the pores of the screen and block the paths for vapor release.

Figure 3.14 shows the average temperatures in the evaporator, $T_{e,m}$, and condenser, $T_{c,m}$, for heat pipe E and heat pipe G with 1.1 ml fill amount in the case of mode 3 heater. The average temperatures in the adiabatic section, $T_{a,m}$, are approximately equal to 90°C. The average condenser temperatures of heat pipe E are lower than those of heat pipe G. The average evaporator temperatures of heat pipe E are slightly higher than those of heat pipe G. As a result, the ΔT_{ec} of heat pipe G is smaller than that of heat pipe E. ΔT_{ec} Values for heat pipe E and heat pipe G at different operating temperatures are given in Table 3.3. It is clearly exhibited by comparison that the thermal performance of heat pipe G is better that of heat pipe E. Comparisons of the average temperatures

38

Figure 3.14   Comparison of the average temperatures in the evaporator and condenser between heat pipe E and heat pipe G with mode 3 heater.

Table 3.3 ΔT_{ec} values for heat pipe E and heat pipe G with 1.1 ml fill amount.

Heater Mode	Heat Pipe	$T_v = 60°C$	$T_v = 80°C$	$T_v = 90°C$	
		$Q_{in} = 50W$	$Q_{in} = 50W$	$Q_{in} = 50W$	$Q_{in} = 60W$
Mode 1	E	41.84	33.21	29.2	36.87
	G	30.48	25.65	24.5	29.92
Mode 2	E			20.4	25.21
	G			17.38	20.53
Mode 3	E	24.81	19.38	16.76	20.97
	G	16.88	13.25	13.15	15.44

in the evaporator, $T_{e,m}$, and condenser, $T_{c,m}$, between heat pipe F and heat pipe G with 1.1 ml fill amount are made in Figure 3.15 for mode 1 heater and Figure 3.16 for mode 2 heater. The average temperatures in the adiabatic section, $T_{a,m}$, are approximately equal to 90°C. The average condenser temperatures of heat pipe G is slightly lower than those of heat pipe F. The average evaporator temperatures of heat pipe G are significantly lower than those of heat pipe F. As a result, the ΔT_{ec} of heat pipe G is smaller than that of heat pipe F. Therefore, in the group of the folded screen, heat pipe G with 1.1 ml fill amount has the best thermal performance.

39
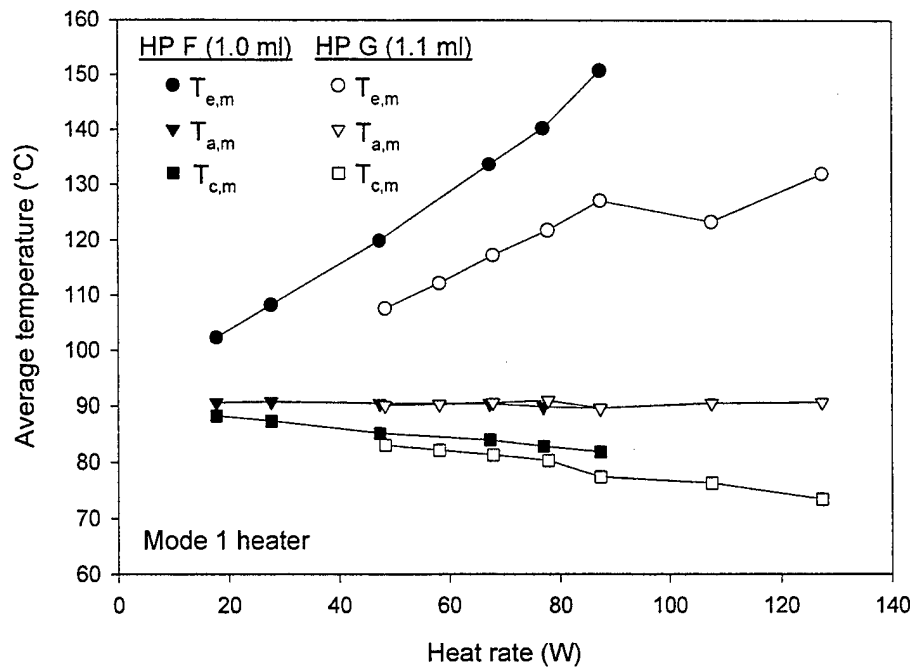
Figure 3.15 Comparison of the average temperatures in the evaporator and condenser between heat pipe F and heat pipe G with mode 1 heater.
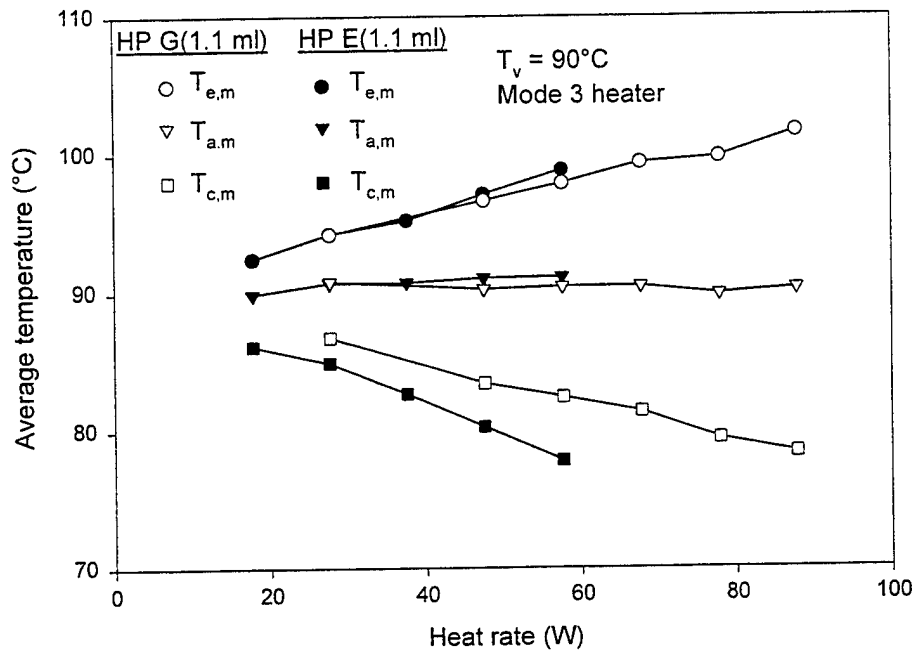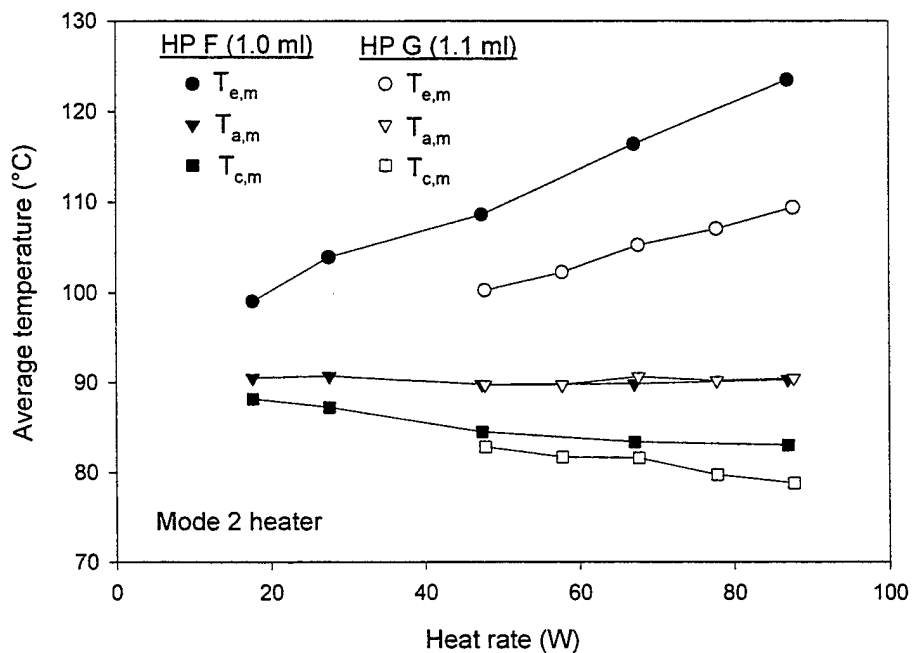

Figure 3.16 Comparison of the average temperatures in the evaporator and condenser between heat pipe F and heat pipe G with mode 2 heater.

40

Test results for heat pipe A with the fill amount of 1.4 ml is shown in Figure 3.17. The value of ΔT_{ec} has already exceeded 68.5°C at a heat rate of 25 W. This indicates that heat pipe A with a folded sheet fin can not operate as heat transfer element.
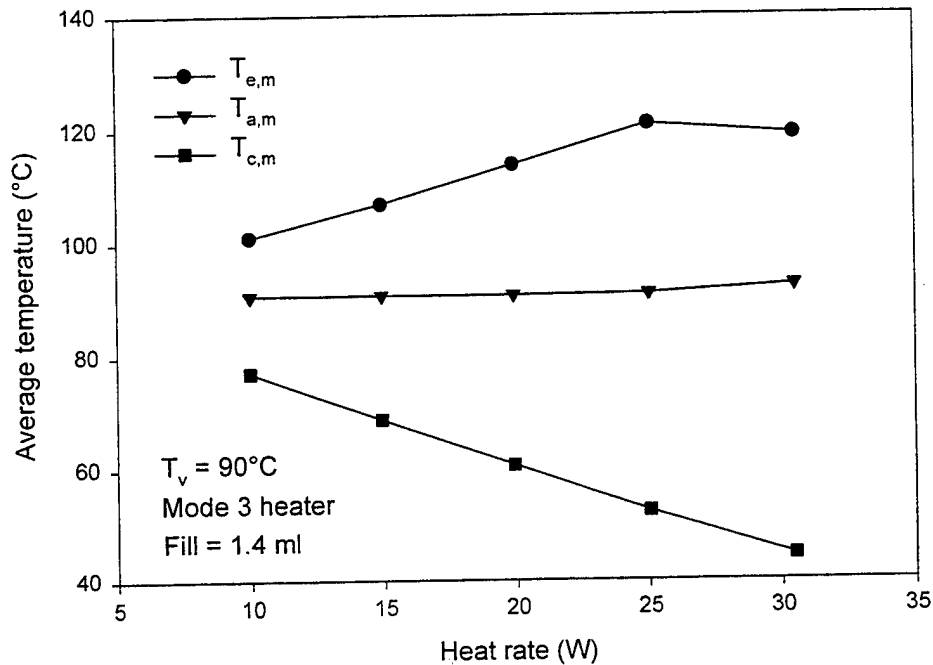
Figure 3.17 Average temperatures vs. the heat rate for heat pipe A with mode 3 heater.

The effect of the working fluid fill amount on the thermal performance of heat pipe G is shown in Figure 3.18. Heat pipe G with three different fill amounts is operated at $T_v = 60$°C using mode 3 heater. The average evaporator temperature for the fill amount of 0.69 ml is much higher than that for other fill amounts indicating an under-fill condition. For the three different fill amounts, the fill amount of 1.1 ml results in the smallest ΔT_{ec} at the tested heat rates greater than 9 W. The use of the stiffener holding the folded screen against the heat pipe wall enhances the thermal contact conductance between the folded screen and the heat pipe wall and hence largely reduces the ΔT_{ec}.
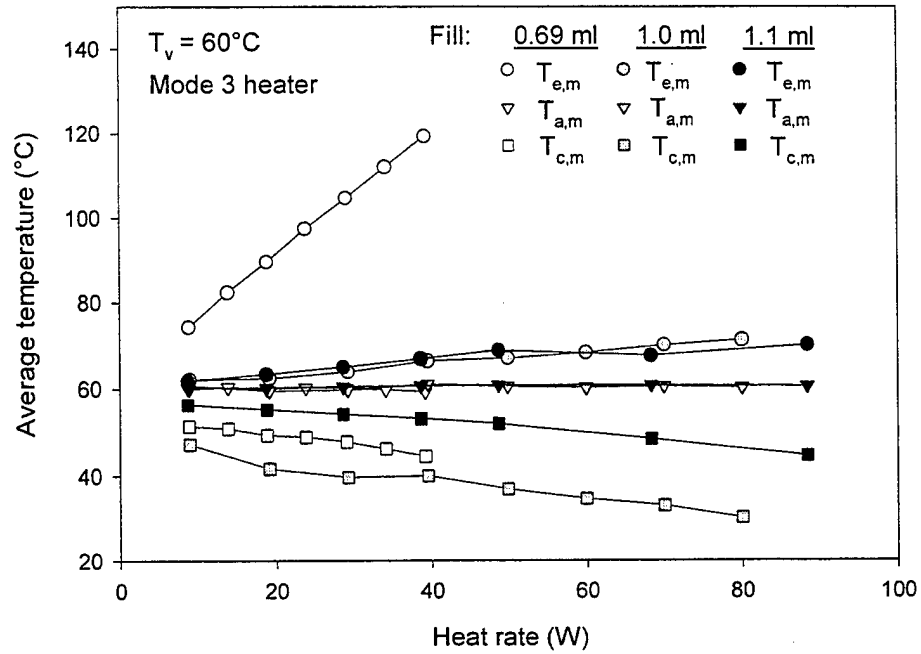
Figure 3.18 Effect of fill amount on the average temperatures in the evaporator and condenser vs. the heat rate for heat pipe G with mode 3 heater.

Figure 3.19 shows the effect of working fluid fill amount on the average temperatures in the evaporator and condenser for heat pipe B with mode 3 heater. The operating temperature is 90°C. It is evident that the average condenser temperature for the 1.3 ml fill amount is much lower than that for the 0.87 ml and the ΔT_{ec} is much smaller for the 0.87 ml than for the 1.3 ml. The reason is that the capillary fin in the condenser is submerged in the working fluid for the case of the 1.3 ml fill amount. The excess liquid above the fin tip results in a lower condensation heat transfer coefficient due to a lower thermal conductivity of the liquid. The fill amount of 0.87 ml is equivalent to a fill ratio of 80% that is defined by the ratio of the working fluid volume to the volume of all the grooves. Because of this result, the fill amount of 0.87 ml or one close to it is used for the capillary fin heat pipes.

Figure 3.19 Effect of fill amount on the average temperatures in the evaporator and condenser vs. the heat rate for heat pipe B with mode 3 heater.

3.4.2 Test results and discussion

3.4.2.1 Axial temperature profiles

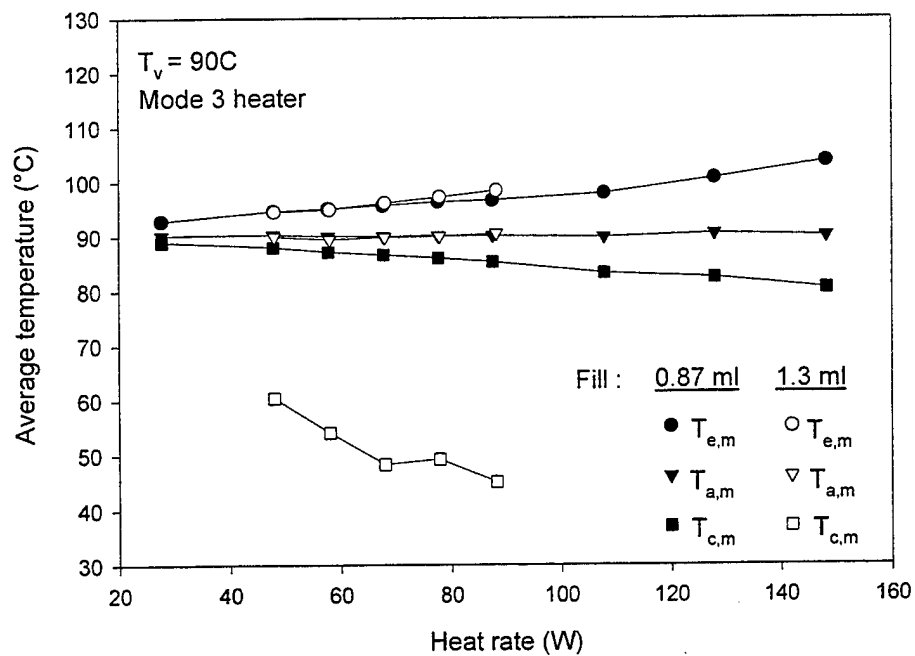Figure 3.20, 3.21 and 3.22 show temperature profiles along the top and bottom surfaces of heat pipe B with the 0.87 ml fill amount at $T_v = 90°C$ for mode 1, mode 2 and mode 3 heating configurations. The input heat rate is varied from 60 W to 150 W. In Figure 3.20 for mode 1 heater, with an increase in the heat rate, the temperatures on the bottom of the evaporator increase and the temperatures in the condenser decrease. The peak temperature at the second thermocouple location where the chip resistor is active increases noticeably with increasing the heat rate. At 110 W, the temperature difference between the peak temperature and the operating temperature reaches 30°C. In Figure 3.21 for mode 2 heater, the evaporator temperatures on the top surface are slightly higher than those on the bottom and the condenser temperatures on the top surface are slightly lower than those on the bottom at the input power level of 60 W, 90 W and 110 W. At 150 W, the peak temperature is greater on the bottom surface than on the top and the temperature difference between the peak temperature and the operating temperature is 22°C. In Figure 3.22 for mode 3 heater, the temperature profiles on the top surface are slightly different from those on the bottom at 60 W, 90 W and 110 W. At 150 W, the temperatures on the bottom surface of the evaporator are noticeably higher than those on the top surface.

Figure 3.23, 3.24 and 3.25 show temperature profiles along the top and bottom surfaces of heat pipe D for mode 1, mode 2 and mode 3 heating configurations. The working fluid fill amount is 0.85 ml. The operating temperature is 90°C. In Figure 3.23, with an increase in the heat rate, the temperatures on the bottom of the evaporator increase, more significantly than on the top, and the temperatures in the condenser decreases. The peak temperature is related to the place of the active chip resistor. At 110 W, the temperature difference between the peak temperature and the operating temperature reaches 30°C similar to the case of heat pipe B (Figure 3.20). In Figure 3.24 and 3.25, the evaporator temperatures on the top surface are slightly higher than those on the bottom and the condenser temperatures on the top surface are slightly lower than those on the bottom for the same input power level. In Figure 3.25, the highest temperature along the heat pipe occurs at the first

thermocouple location for the same input power level.

Figure 3.26 and 3.27 show temperature profiles along the top and bottom surfaces of heat pipe G with the 1.1 ml fill amount for mode 1 and mode 3 heating configurations. The operating temperature is 90°C. In Figure 3.26, the trend of the temperature increases on the bottom and top of the evaporator is qualitatively similar to the case of heat pipe B. At 90 W, the temperature difference between the peak temperature and the operating temperature reaches 37°C, much higher than the case of heat pipe B (shown in Figure 3.20). In Figure 3.27, the evaporator temperatures on the top surface are approximately the same as on the bottom and the condenser temperatures on the top surface are lower than those on the bottom for the same input power level. The highest temperature along the heat pipe occurs at the first thermocouple location for the same input power level.
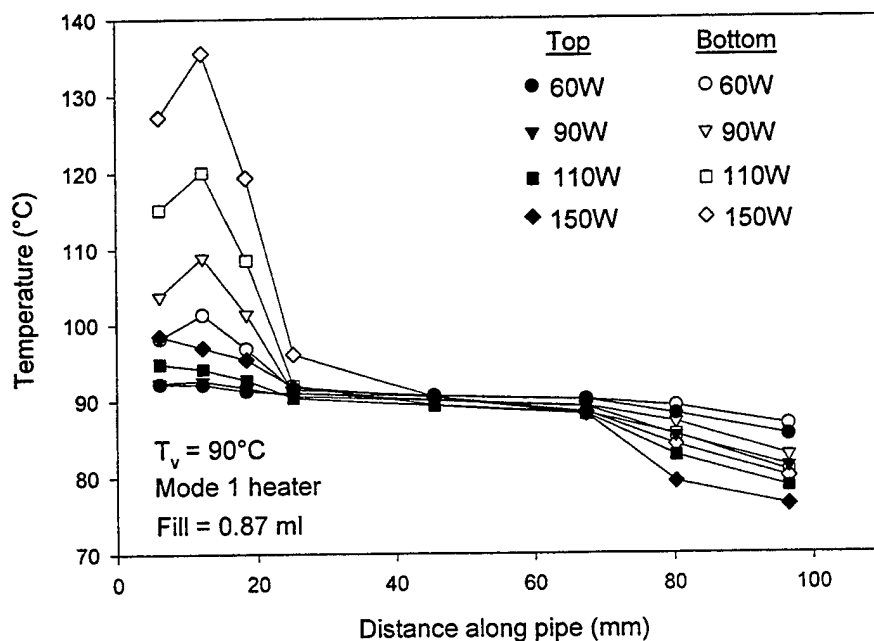
Figure 3.20   Temperature profiles along the top and bottom surfaces of heat pipe B with 0.87 ml fill amount for mode 1 heater.
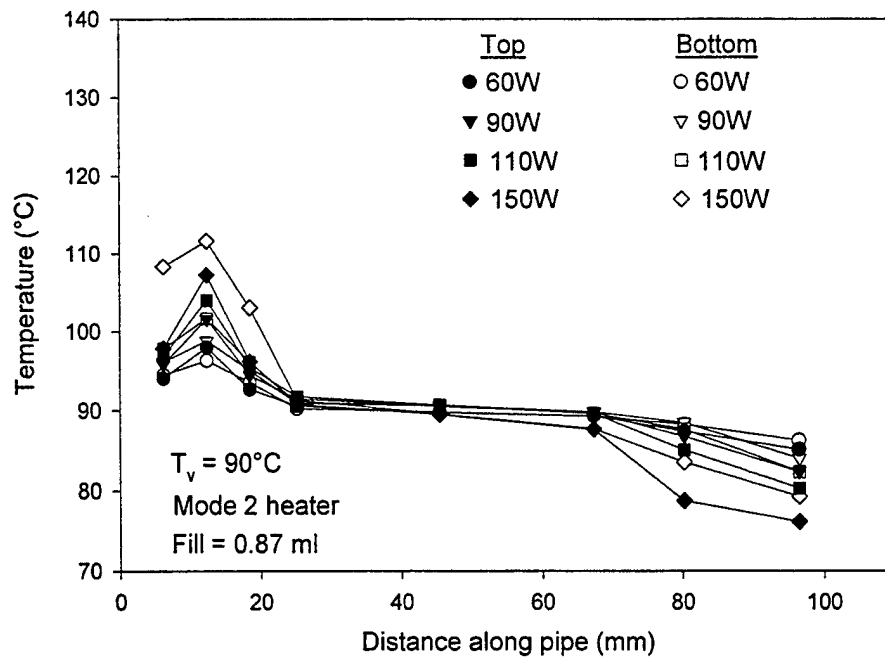
Figure 3.21   Temperature profiles along the top and bottom surfaces of heat pipe B with 0.87 ml fill amount for mode 2 heater.
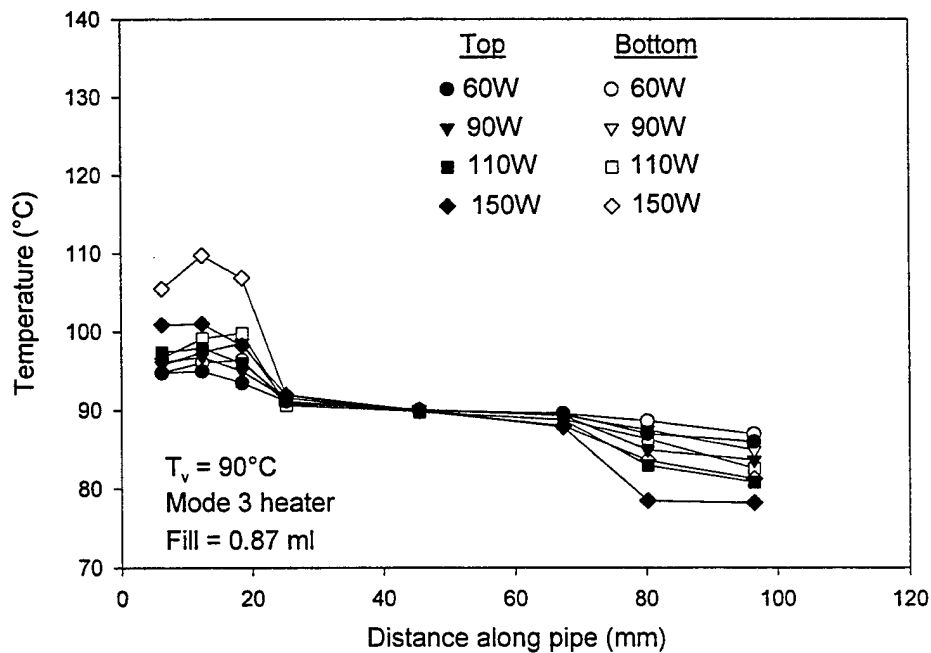
Figure 3.22   Temperature profiles along the top and bottom surfaces of heat pipe B with 0.87 ml fill amount for mode 3 heater.
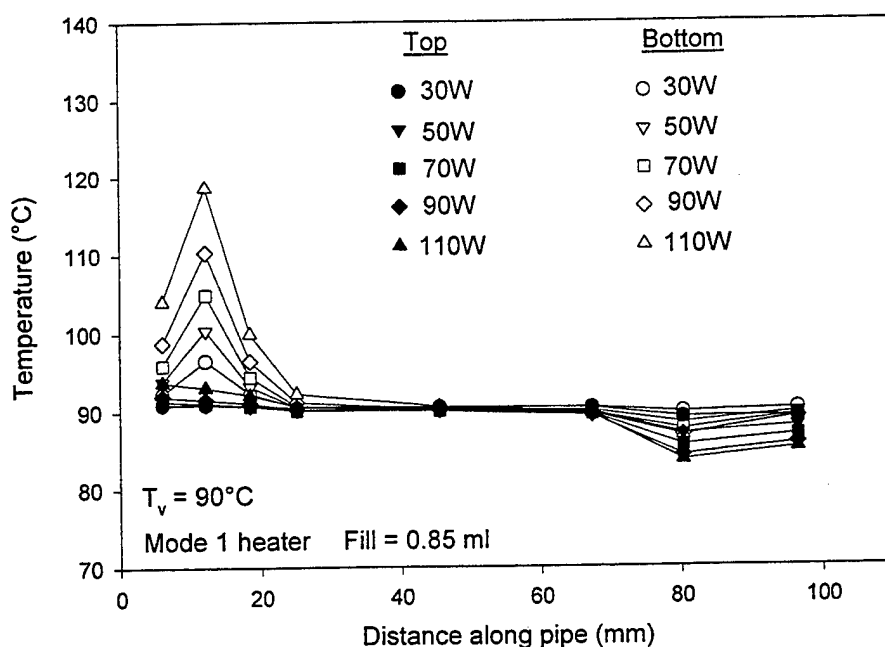
Figure 3.23   Temperature profiles along the top and bottom surfaces of heat pipe D with 0.85 ml fill amount for mode 1 heater.
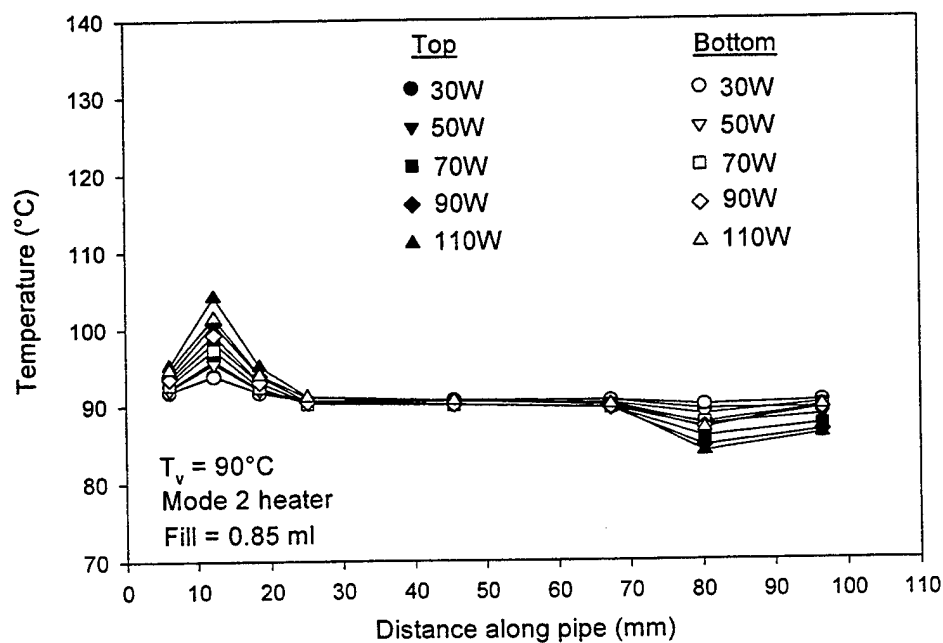
Figure 3.24   Temperature profiles along the top and bottom surfaces of heat pipe D with 0.85 ml fill amount for mode 2 heater.
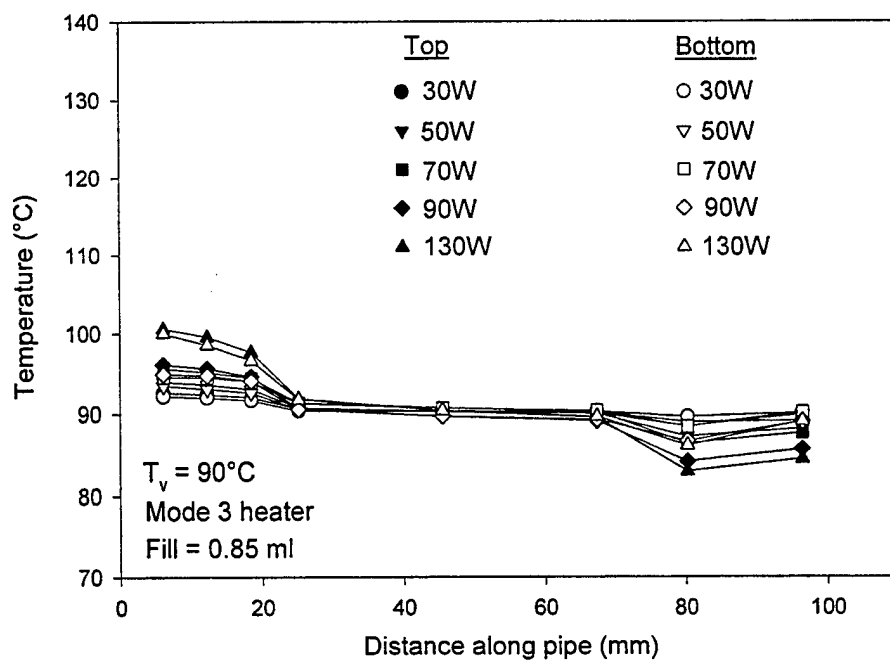
Figure 3.25   Temperature profiles along the top and bottom surfaces of heat pipe D with 0.85 ml

fill amount for mode 3 heater.
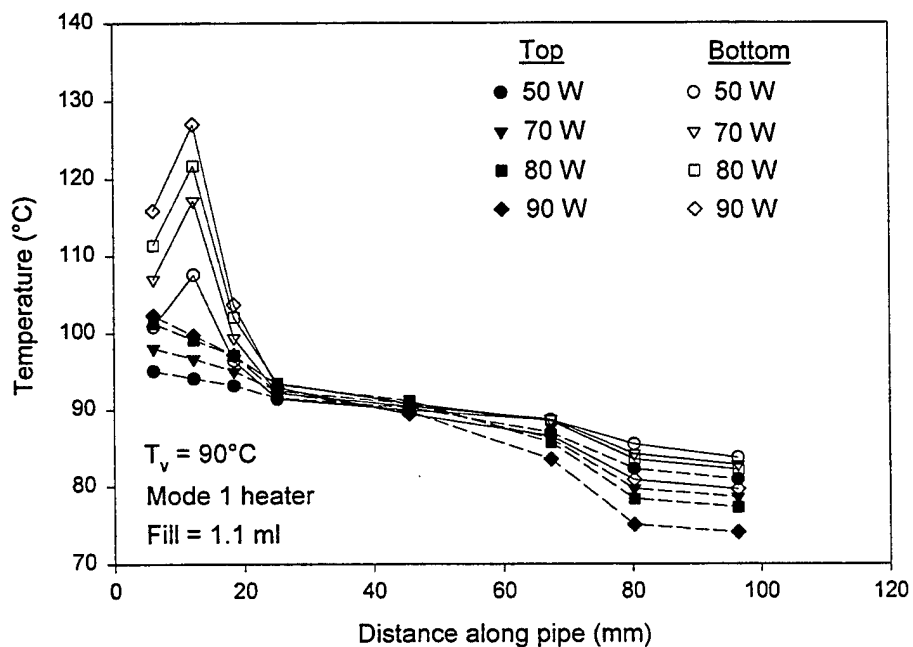
Figure 3.26   Temperature profiles along the top and bottom surfaces of heat pipe G with 1.1 ml

fill amount for mode 1 heater.
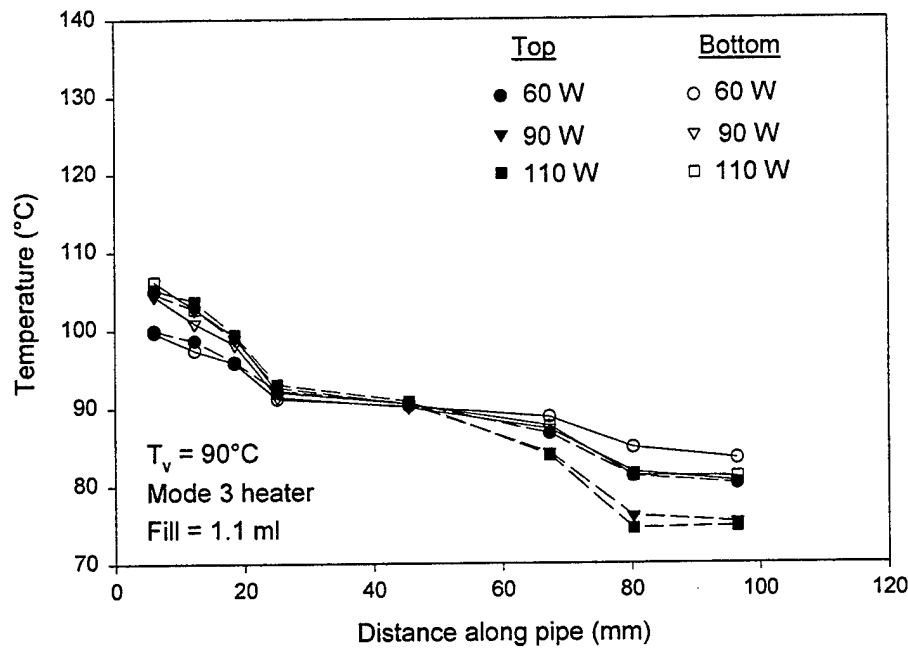
Figure 3.27   Temperature profiles along the top and bottom surfaces of heat pipe G with 1.1 ml

fill amount for mode 3 heater.

3.4.2.2 Heat transfer coefficients

To estimate the heat transfer characteristic of the heat pipes, the evaporator and condenser heat transfer coefficients are defined as follows:

$$h_e = \frac{Q}{A_h(T_{e,i,m} - T_{a,m})}$$

$$h_c = \frac{Q}{A_c(T_{a,m} - T_{c,i,m})}$$

where the inner wall average temperatures of the evaporator and condenser are calculated as follows:

$$T_{e,i,m} = T_{e,m} - \frac{Qt_w}{A_h k_w}$$

$$T_{c,i,m} = \frac{Qt_w}{A_c k_w} + T_{c,m}$$

where Q is the heat rate, A_h the heating surface area dependent on the chip resistor arrangement, A_c

the cooling surface area ($A_c=2L_cB_1$), t_w the heat pipe wall thickness (1.22 mm), and k_w the thermal conductivity of the wall material (390 W/mK).

Figure 3.28, 3.29 and 3.30 show heat transfer coefficients of evaporator (h_e) and condenser (h_c) of heat pipe B with the 0.87 ml fill amount for mode 1, mode 2 and mode 3 heating configurations. The heat transfer coefficients are related with the heat rate and operating temperature. In Figure 3.28 and 3.29, the value of h_c at the operating temperature of 60°C and 80°C does not change much with a variation of the heat rate. The value of h_c decreases slightly with an increase in the heat rate at 90°C and 110°C. Given a heat rate, an increase in the operating temperature results in a slight increase in h_c. Most condenser heat transfer coefficients vary between 19000 W/m^{2}K and 33000 W/m^{2}K. In Figure 3.28, the evaporator heat transfer coefficient has the maximum value at the operating temperature of 60°C, 80°C and 90°C. The maximum value occurs at a higher heat rate with an increase in the operating temperature up to 90°C. At the operating temperatures of 80°C and 90°C, the maximum h_e is 123000 and 121000 W/m^{2}K. In Figure 3.29, the evaporator heat transfer coefficient reaches its maximum value of 74200 W/m^{2}K at 69 W for 60°C, 82600 W/m^{2}K at 88 W for 80°C, 71000 W/m^{2}K at 88 W for 90°C, and 70700 W/m^{2}K at 97.5 W for 110°C. The maximum values of h_e do not vary much with the operating temperature. In Figure 3.30, the value of h_c decreases with an increase in the heat rate especially at the operating temperature of 80°C, 90°C and 110°C. In a similar manner, the evaporator heat transfer coefficient has the maximum value at the operating temperature of 60°C, 80°C, 90°C and 110°C, and the maximum h_e occurs at a higher heat rate if the operating temperature is increased. At the operating temperature between 60°C and 110°C, the maximum h_e changes between 29700 W/m^{2}K to 34900 W/m^{2}K.

Figure 3.31, 3.32 and 3.33 show heat transfer coefficients of evaporator and condenser of heat pipe D with the 0.85 ml fill amount for mode 1, mode 2 and mode 3 heating configurations. The heat transfer coefficients are plotted as a function of the heat rate for different operating temperatures. Given an operating temperature, the value of h_c does not change much with a variation of the heat rate though a slight decrease in h_c is found with an increase in the heat rate at the operating temperatures of 90°C and 110°C. Given a heat rate, the value of h_c is higher at 80°C than at 90°C. However, the lowest value of h_c is found at 60°C and the highest at 110°C at a given heat rate. Most condenser heat transfer coefficients vary between 40000 W/m^{2}K and 73000 W/m^{2}K. By contrast

50

with heat pipe B, the maximum value of h_e is not noticeable for the same operating temperature. In Figure 3.31, at the heat rate greater than 48 W, the value of h_e decreases slightly with an increase in the heat rate. In Figure 3.32, the value of h_e does not change much at 80°C, 90°C and 110°C though it decreases with an increase in the heat rate at 60°C. For the operating temperatures of 80°C, 90°C and 110°C, the value of h_e varies between 61000 W/m²K and 75000 W/m²K. In Figure 3.33, the value of h_e does not change much at 80°C, 90°C and 110°C. At 60°C, the value of h_e decreases as the heat rate is varied from 49 W to 109 W. For the operating temperatures of 80°C, 90°C and 110°C, the value of h_e varies between 36000 W/m²K and 47500 W/m²K.

Figure 3.34 and 3.35 show heat transfer coefficients of evaporator and condenser of heat pipe G with the 1.1 ml fill amount for mode 1 and mode 3 heating configurations. In a similar manner, given an operating temperature, the value of h_c does not change much with a variation of the heat rate. The lowest value of h_c is found at 60°C and the highest at 110°C. Most condenser heat transfer coefficients vary between 7000 W/m²K and 14700 W/m²K for the heat rates greater than 30 W. The maximum value of h_e is not noticeable for the same operating temperature. The value of h_e does not change much for the same operating temperature. The value of h_e varies between 28100 W/m²K and 57000 W/m²K for mode 1 heater and between 16400 W/m²K and 25400 W/m²K for mode 3 heater.

Figure 3.28   Heat transfer coefficients of evaporator and condenser of heat pipe B with 0.87 ml fill amount for mode 1 heater.

Figure 3.29   Heat transfer coefficients of evaporator and condenser of heat pipe B with 0.87 ml fill amount for mode 2 heater.

52
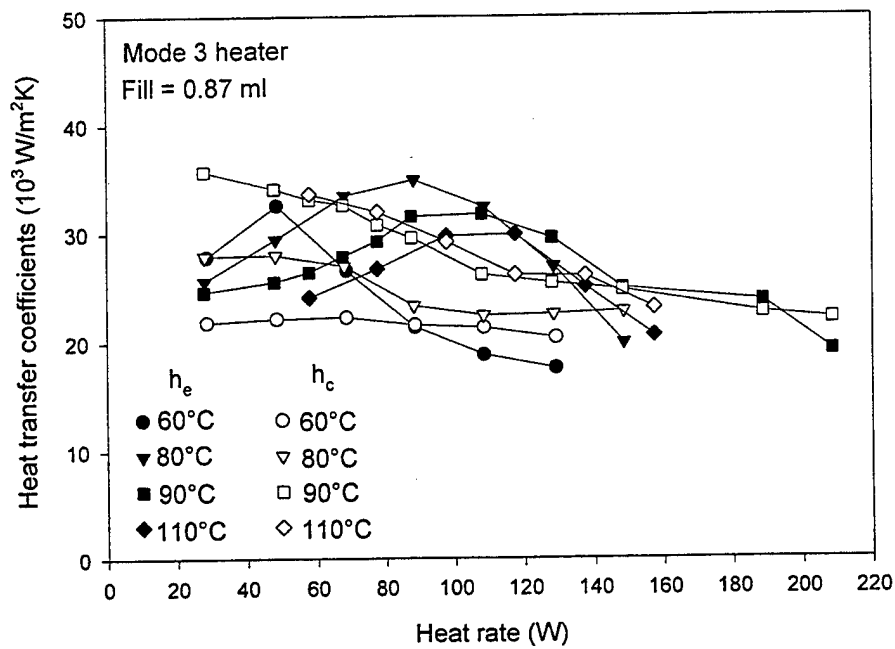
Figure 3.30   Heat transfer coefficients of evaporator and condenser of heat pipe B with 0.87 ml fill amount for mode 3 heater.
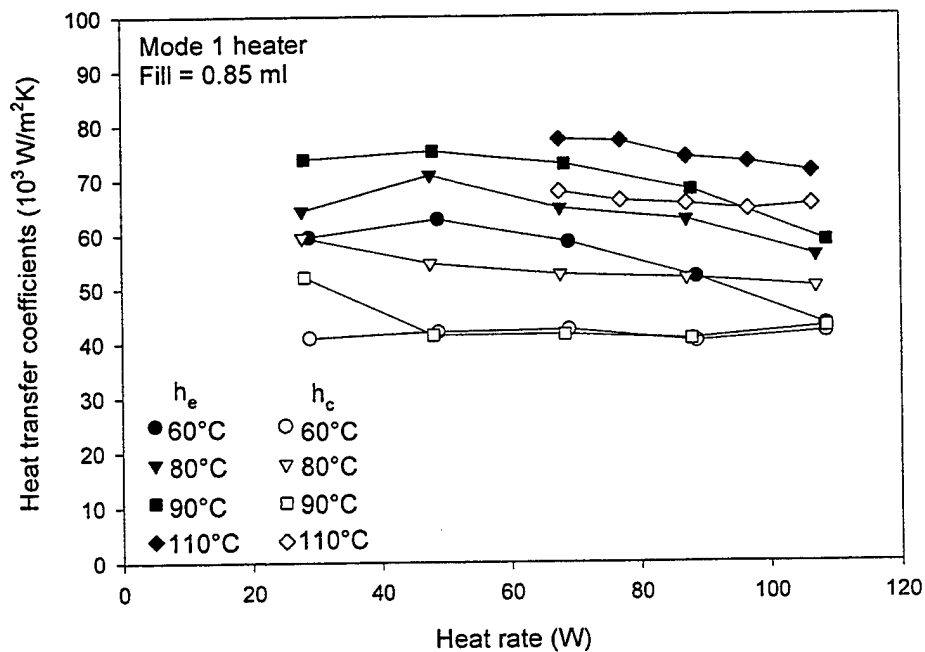
Figure 3.31   Heat transfer coefficients of evaporator and condenser of heat pipe D with 0.85 ml fill amount for mode 1 heater.

53
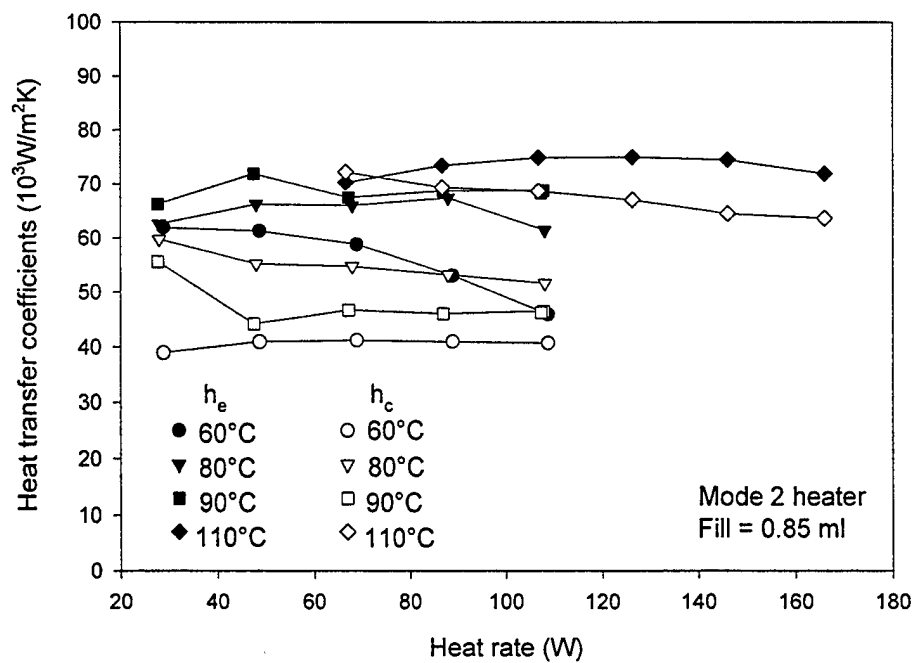
Figure 3.32   Heat transfer coefficients of evaporator and condenser of heat pipe D with 0.85 ml fill amount for mode 2 heater.
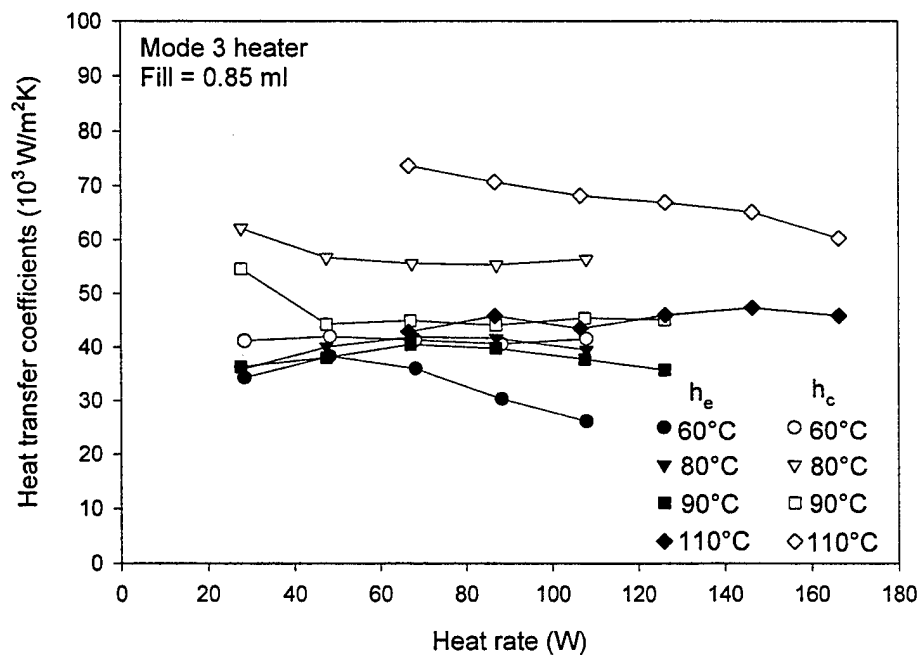
Figure 3.33   Heat transfer coefficients of evaporator and condenser of heat pipe D with 0.85 ml fill amount for mode 3 heater.
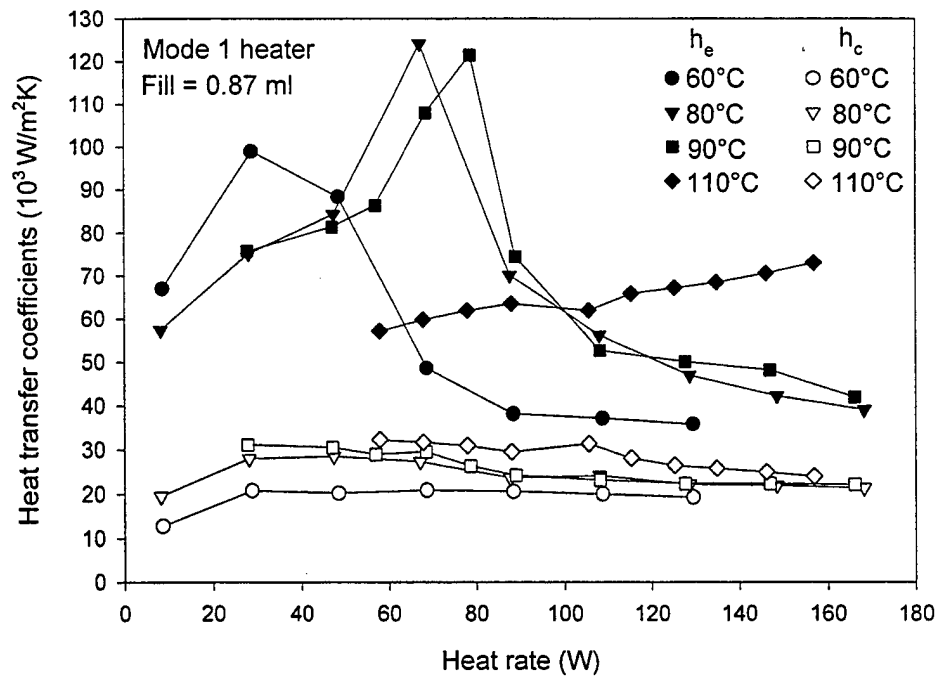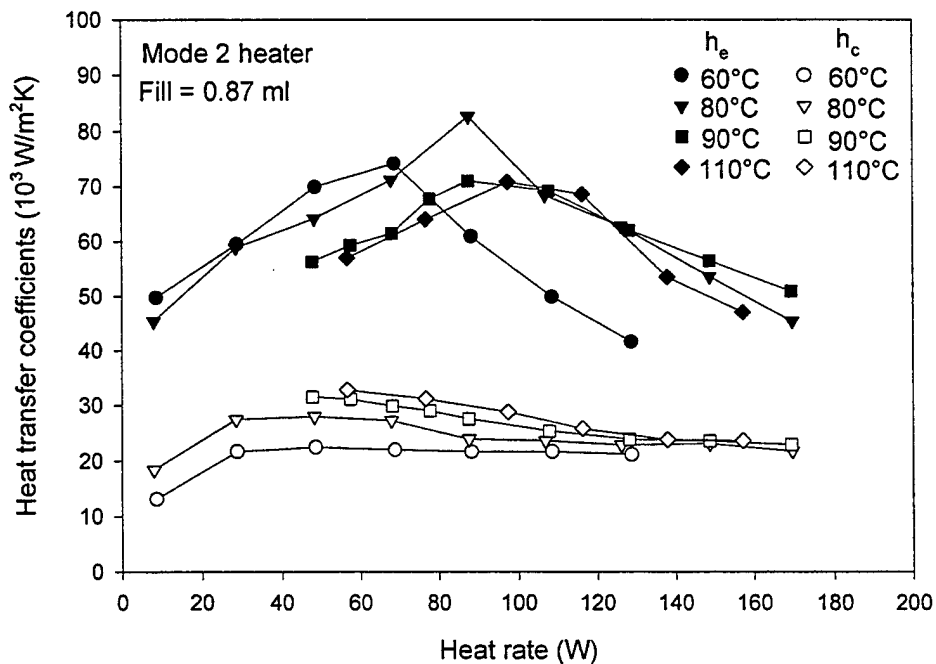
54
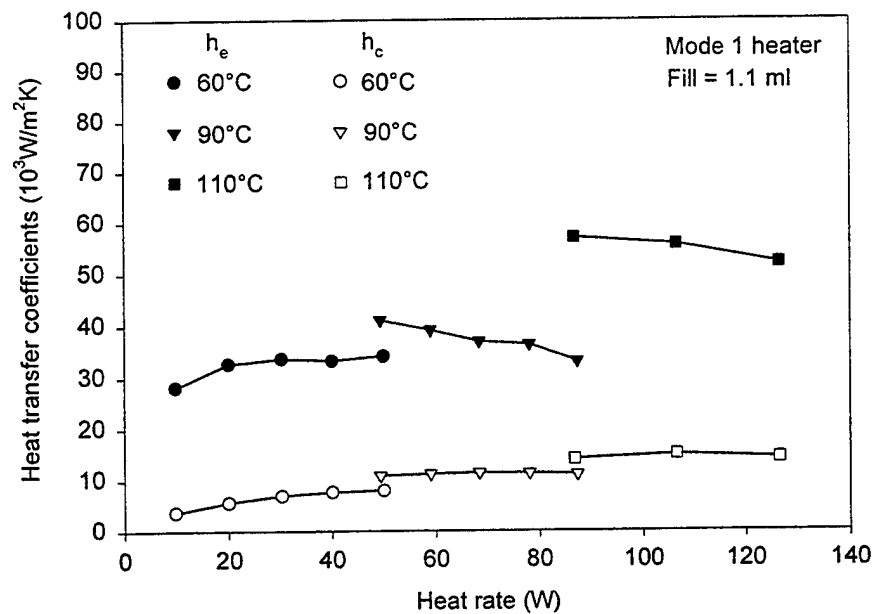
Figure 3.34   Heat transfer coefficients of evaporator and condenser of heat pipe G with 1.1 ml fill amount for mode 1 heater.
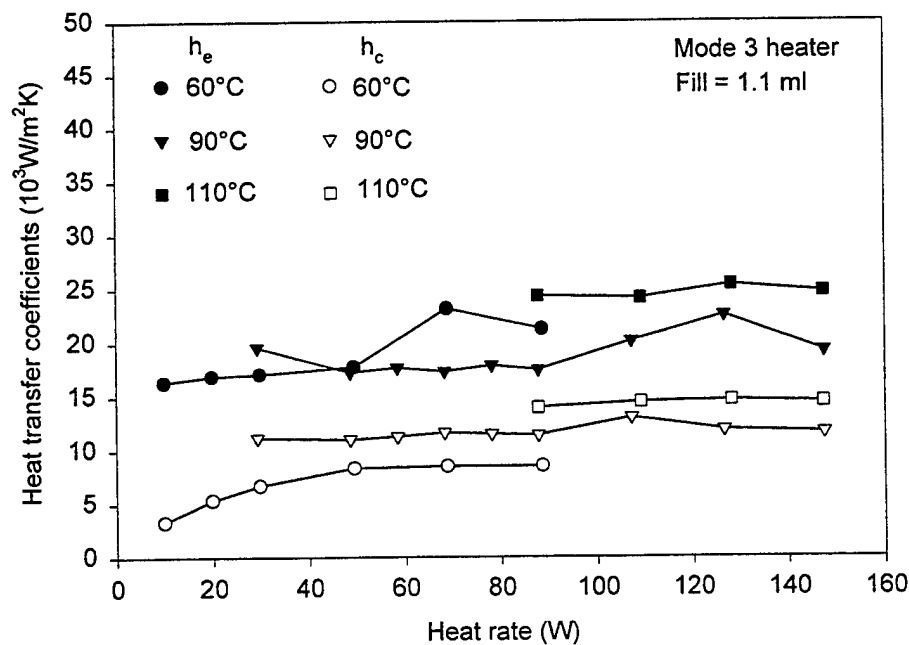
Figure 3.35   Heat transfer coefficients of evaporator and condenser of heat pipe G with 1.1 ml fill amount for mode 3 heater.

55

3.4.2.3 Effect of condenser cooling rate

Figure 3.36 shows a ratio of the heat rate through the top cooler to that through the bottom cooler for heat pipe B with the 0.87 ml fill amount. The heat rate ratio is presented as function of the input power for the operating temperatures of 80°C and 110°C and for the heating configurations of mode 2 and mode 3. In most cases, the heat rate ratios for mode 2 heater and for mode 3 heater are approximately the same for the same operating temperature. The operating temperature does have an effect on the heat rate ratio. At 80°C, the heat rate ratio decreases from 1.6 to 1.25 with the input power increased from 90 W to 150 W. At 110°C, the heat rate ratio decreases from 1.0 to 0.75 with the input power increased from 80 W to 160 W. The heat rate ratio is greater at 80°C than at 110°C. This may be attributed to a coupled effect of the surface tension and gravity on the curvature of liquid-vapor interface.
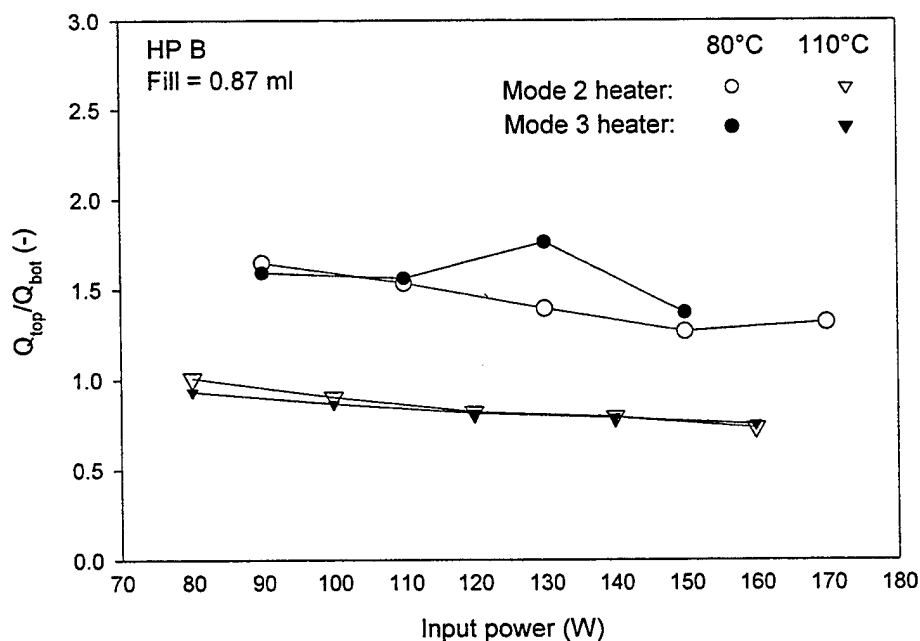
Figure 3.36   Ratio of the heat rate through the top cooler to that through the bottom cooler for heat pipe B with 0.87 ml fill amount.

3.4.2.4 Comparison with literature data

The thermal performance of heat pipe B is compared with that of a heat pipe found in Ref 11. Figure 3.37 shows a cross-sectional view of the Ref 11 heat pipe. Figure 3.38 shows temperatures of three thermocouples in the evaporator, condenser and adiabatic section for heat pipe B and for the Ref 11 heat pipe. The heat pipes are operated with mode 2 heater at 90°C. Thermocouples of the Ref 11 heat pipe are located at the corner of the heat pipe. The temperatures of $T_{e,c}$, $T_{a,c}$ and $T_{c,c}$ are related to an evaporator location close to the end cap, a location in the middle adiabatic section, and a condenser location close to the end cap. The evaporator temperature, adiabatic temperature and condenser temperature of present heat pipe B are related to the first, fifth and eighth thermocouples counted from the evaporator end. The temperatures of $T_{e,u}$, $T_{a,u,}$ and $T_{c,u}$ are located on the top surface and $T_{e,l}$, $T_{a,l,}$ and $T_{c,l}$ on the bottom surface. In most cases, given a heat rate, the temperature difference between the evaporator and the condenser is slightly greater for the reported heat pipe than for the present heat pipe B (on either the top surface or the bottom surface). Although the thermocouple locations and the heating boundary of heat pipe B are somewhat different from those of the Ref 11 heat pipe, the information provided in Figure 3.38 indicates that the thermal performance of heat pipe B is better than that of the Ref 11 heat pipe.
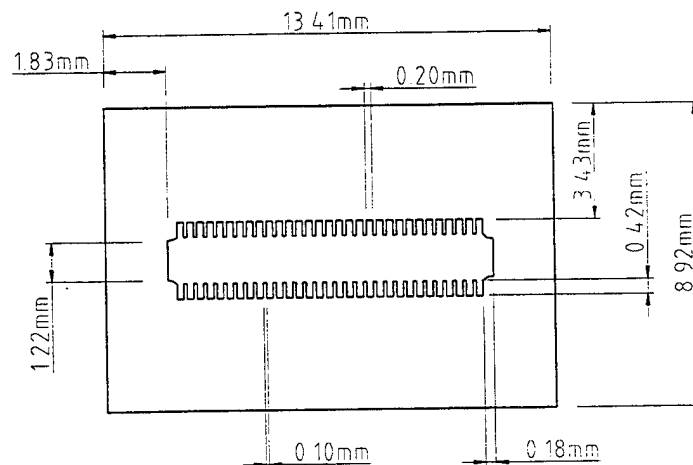
Figure 3.37 Cross-sectional view of the Ref 11 MHP.
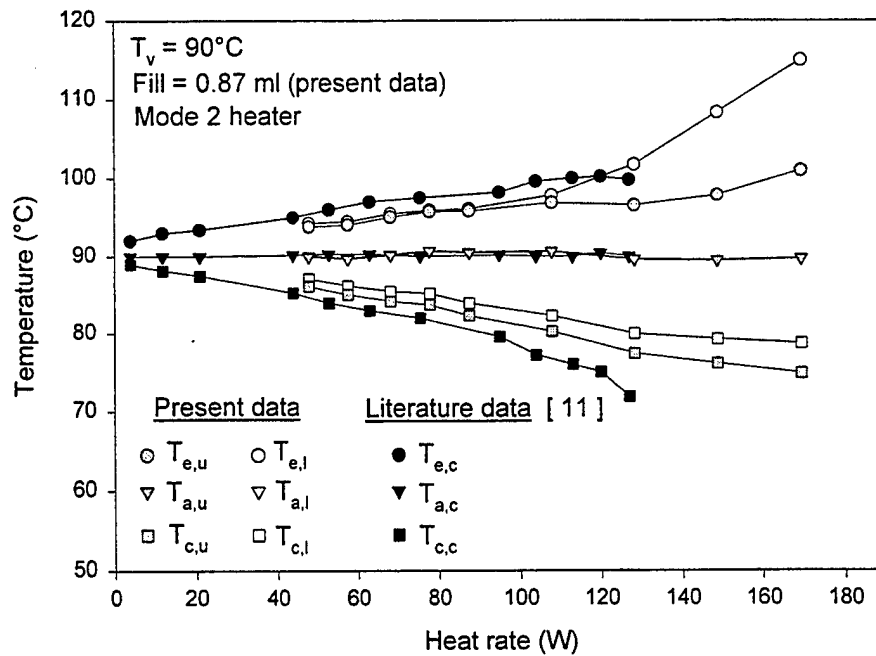
Figure 3.38 Comparison of the temperatures of heat pipe B with 0.87 ml fill amount with literature data.[11]

3.4.2.5 Comparison of thermal performances between folded sheet fin and folded screen heat pipes

Figure 3.39, 3.40 and 3.41 show the average temperatures in the evaporator and condenser of heat pipe B and heat pipe G vs. the heat rate for mode 1, mode 2 and mode 3 heating configurations. The operating temperature is 90°C. The fill amount is 0.87 ml for heat pipe B and 1.1 ml for heat pipe G. In all these figures, the temperature difference ΔT_{ec} between the average evaporator temperature and condenser temperature increases with a rise of the heat rate. The values of ΔT_{ec} are smaller for heat pipe B than for heat pipe G at the tested heat rates. The reason is that there is an additional thermal contact resistance between the screen wick and heat pipe wall for heat pipe G and the effective thermal conductivity of the saturated screen wick is smaller than that of the capillary fin. In Figure 3.39, the value of ΔT_{ec} reaches 24°C for heat pipe B and 49.5°C for heat pipe G at the heat rate of 88 W which corresponds to a heat flux of 113 W/cm^2. In Figure 3.40, the value of ΔT_{ec} reaches 14.0°C for heat pipe B and 30.5°C for heat pipe G at the heat rate of 88 W which

58

corresponds to a heat flux of 56.6 W/cm². In Figure 3.41, the value of ΔT_{ec} is 23.0°C for heat pipe B and 36.2°C for heat pipe G at the heat rate of 148 W which corresponds to a heat flux of 32 W/cm². For heat pipe B, given a ΔT_{ec} of 14°C, it is found that the corresponding heat flux is 87.5 W/cm² for mode 1 heater, 56.6 W/cm² for mode 2 heater and 23.2 W/cm² for mode 3 heater. It is concluded that among the three modes of chip resistor arrangement, the highest heat flux at a given value of ΔT_{ec} is obtained in the case of mode 1 heater and the highest heat rate is obtained for mode 3 heater.

Figure 3.39   Comparison of the average temperatures in the evaporator and condenser vs. the heat rate between heat pipe B and heat pipe G for mode 1 heater.

Figure 3.40   Comparison of the average temperatures in the evaporator and condenser vs. the heat rate between the heat pipe B and heat pipe G for mode 2 heater.

Figure 3.41   Comparison of the average temperatures in the evaporator and condenser vs. the heat rate between the heat pipe B and heat pipe G for mode 3 heater.
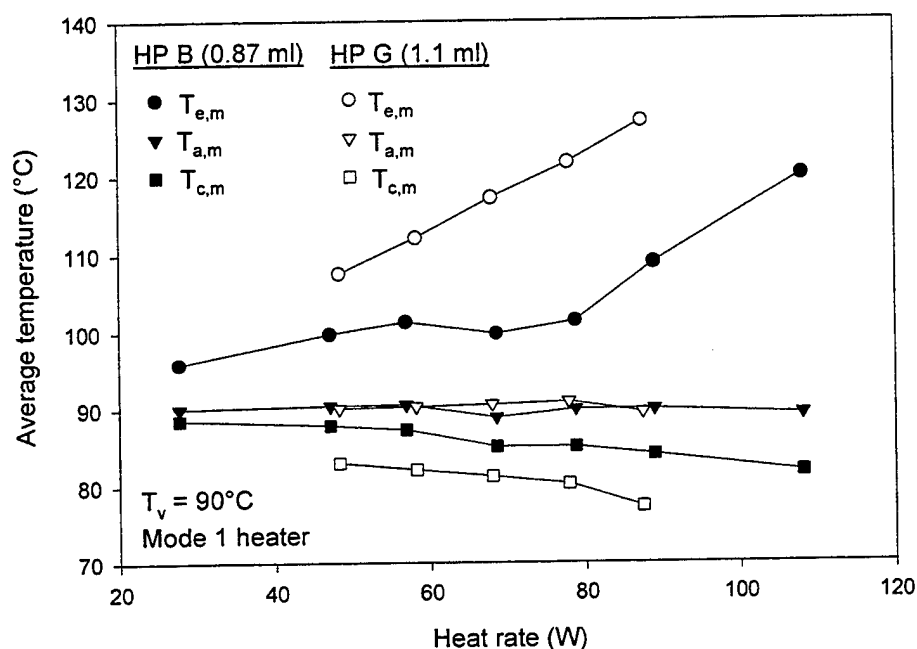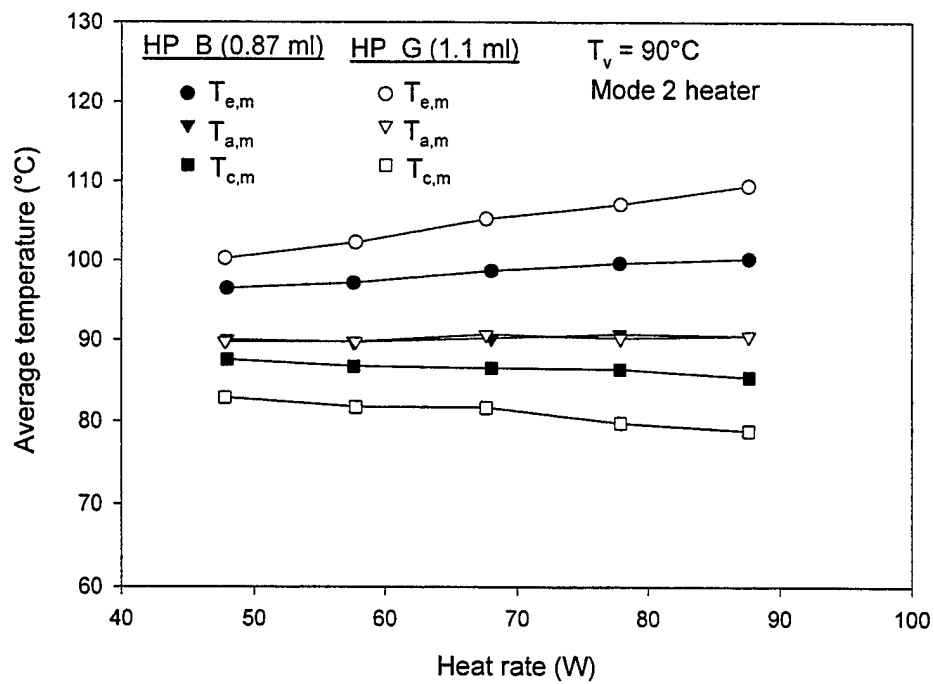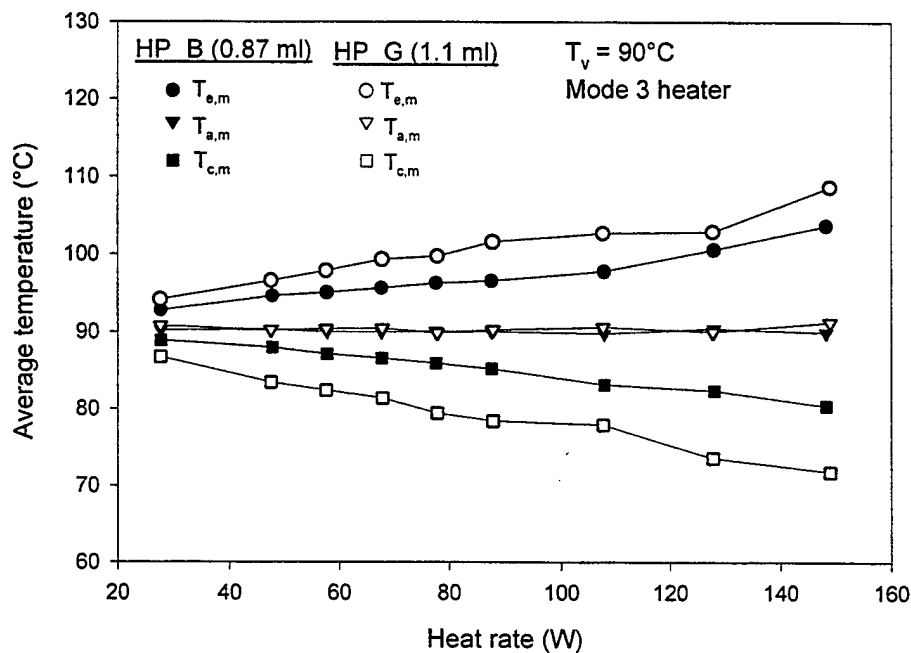
3.4.2.6 <u>Comparison of thermal performances between unnotched and notched folded sheet fin</u>

      <u>heat pipes</u>

Comparison of the thermal performance between heat pipe D and heat pipe B is made in Figure 3.42, 3.43, 3.44 and 3.45. Figure 3.42 shows the comparison of the heat transfer coefficient of evaporator between heat pipe D and heat pipe B at the operating temperatures of 60°C, 90°C and 110°C for mode 2 heater. The profiles of h_e for heat pipe D do not have the noticeable crest while those for heat pipe B have it. At 60°C, most values of h_e are higher for heat pipe B than for heat pipe D. At 110°C, the values of h_e are higher for heat pipe D than for heat pipe B. For the high heat rate, e.g., higher than 127 W, the value of h_e is significantly greater for heat pipe D than for heat pipe B. Figure 3.43 shows the comparison of the heat transfer coefficient of evaporator between heat pipe D and heat pipe B for mode 3 heater. It is clear that the evaporator heat transfer coefficients are greater for heat pipe D than for heat pipe B for the same operating temperature of 60°C, 90°C and 110°C. In the range of the tested heat rate, the increase in h_e for heat pipe D is varied upward from 17% to 95% in comparison with heat pipe B. A larger increase occurring at operating temperature of 110°C. Figure 3.44 shows the comparison of the heat transfer coefficient of condenser between heat pipe D and heat pipe B at 60°C, 90°C and 110°C for mode 2 heater. It is evident that the condenser heat transfer coefficients are greater for heat pipe D than for heat pipe B. The heat transfer enhancement is more significant at 110°C. The value of h_c for heat pipe D is increased by 123% or greater at 110°C in comparison with heat pipe B. Figure 3.45 shows the comparison of the heat transfer coefficient of condenser between heat pipe D and heat pipe B for mode 3 heater. Like the case with mode 2 heater, the condenser heat transfer coefficients are noticeably greater for heat pipe D than for heat pipe B. At 110°C, the value of h_c is enhanced by 120% or greater.

      The fin bridges (the uncut part) existing at the top of the folded sheet fin partially separate the liquid flow from the vapor flow and reduce the average counter-current flow shear stress at the liquid-vapor interface. To some extent, this helps the evaporator be sufficiently wetted by the liquid flowing back through the grooves. At high heat rate, the fin bridges protect the return liquid against being torn from the capillary fin. The fin bridges in the condenser serve as additional secondary heat transfer surfaces and contribute to the enhancement of condensation heat transfer. As a result, heat

pipe D is superior to heat pipe B in the thermal performance. At high temperatures, part of the condensate on the upper fin surface (on the top cooler side) may be drained down to the fin bridges forming a liquid retention region due to gravity. Meanwhile, liquid droplets under the liquid retention region come off the fin and fall onto the bottom surface. The rest of the condensate in the upper inverted grooves flows back to the upper evaporator by the capillary pumping head. With the condensate in part being drained off, a portion of the upper fin surface is exposed and the condensation heat transfer is improved. This explains why the use of the folded sheet fin with notch cuts brings about more significant enhancement of the condensation heat transfer in heat pipe D at the higher operating temperature such as 110°C.

The heat pipe thermal performance at high heat fluxes is investigated with mode 1 and mode 2 heaters. Table 3.4 shows the average temperatures in the evaporator ($T_{e,m}$) and condenser ($T_{c,m}$) of heat pipe D and heat pipe B with mode 2 heater at high heat fluxes greater than 80 W/cm². The operating temperature is varied from 60°C to 110°C. The average condenser temperatures are greater for heat pipe D than for heat pipe B at the same heat fluxes. This means that the condenser heat transfer coefficient is still greater for heat pipe D than for heat pipe B at the high heat fluxes. The average temperatures of the evaporator are smaller for heat pipe D than for heat pipe B, indicating that the evaporator heat transfer coefficient is higher for heat pipe D than for heat pipe B. It is a fact that the high heat flux brings about a larger ΔT_{ec}. The value of ΔT_{ec} decreases with an increase in the operating temperature. For heat pipe D, as an example, the value of ΔT_{ec} reaches 36.09°C at the operating temperature of 90°C and heat flux of 127 W/cm², and decreases to 34.4°C at 100°C, even at a higher heat flux of 141 W/cm².

Table 3.4   Comparison of the average temperatures between heat pipe D and heat pipe B for mode 2 heater at high heat fluxes.

T_v (°C)	Q (W)	q_e(W/cm²)	$T_{e,m}$ (°C)		$T_{c,m}$ (°C)		ΔT_{ec} (°C)	
			HP B (0.87 ml)	HP D (0.85 ml)	HP B (0.87 ml)	HP D (0.85 ml)	HP B (0.87 ml)	HP D (0.85 ml)
60	125	80.4	90.67	82.63	50.13	54.36	40.54	28.27
80	172	111	122.21	114.53	67.68	73.58	54.53	40.95
90	198	127	136.93	119.6	76.69	83.51	60.24	36.09
100	219	141	139.76	126.62	84.93	92.22	54.83	34.4
110	244	157	152.41	126.40	93.90	102.88	58.51	23.52

Very high heat fluxes can be achieved using mode 1 heater. During the experiment with mode 1 heater, no temperature excursion on the evaporator wall of the heat pipe has been found in the operating temperature range between 60°C and 100°C even if the heat flux is increased up to 283 W/cm² at 100°C and to 158 W/cm² at 60°C. This means that the heat pipe is still operating in the quasi-steady state. However, the peak evaporator temperature has reached 170.4°C for $T_v = 100$°C and 112.6°C for $T_v = 60$°C. Meanwhile, the average condenser temperature is 92.4°C for $T_v = 100$°C and 55.1°C for $T_v = 60$°C. Apparently, the heat pipe has lost its commonly addressed advantages due to the high temperature difference between its peak evaporator temperature and operating temperature though its maximum performance has not been encountered. This feature pertains to the spot heated heat pipe with a heating area as small as 0.774 cm². In this case, the temperature difference between the peak temperature and operating temperature is a more critical parameter to evaluate the performance of the heat pipe. It is possible to design a high heat flux heat pipe with a small heating area, but the price for the operation at the very high heat flux is a resultant large ΔT_{ec} across the heat pipe length. The objective of developing high performance heat pipes is to reduce their internal thermal resistance at the high heat flux.

Figure 3.42   Comparison of the heat transfer coefficient of evaporator between heat pipe D and heat pipe B at three different operating temperatures for mode 2 heater.

Figure 3.43   Comparison of the heat transfer coefficient of evaporator between heat pipe D and heat pipe B at three different operating temperatures for mode 3 heater.

64

Figure 3.44 Comparison of the heat transfer coefficient of condenser between heat pipe D and heat pipe B at three different operating temperatures for mode 2 heater.
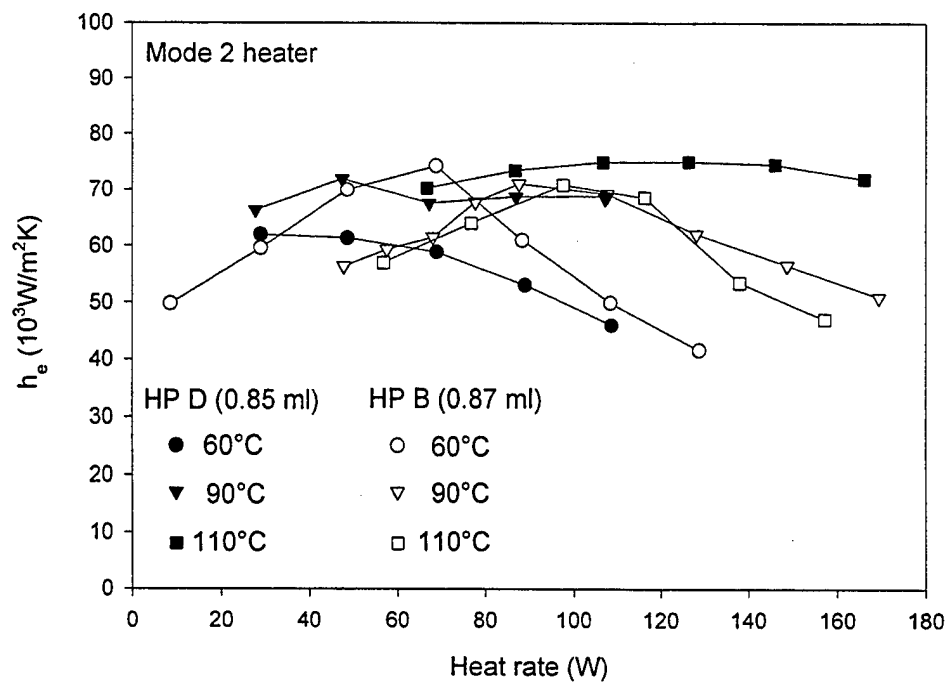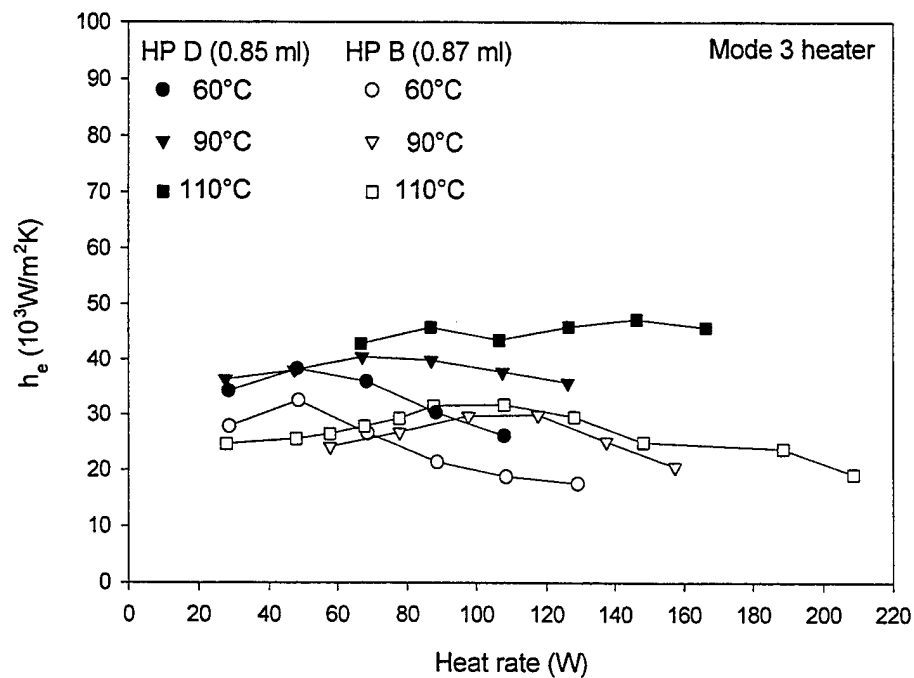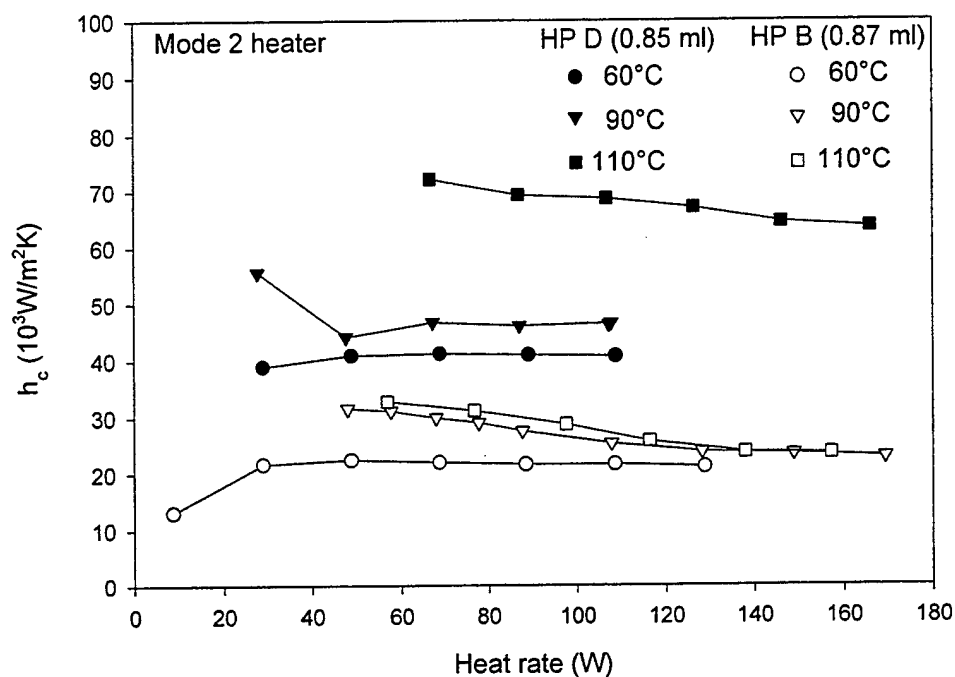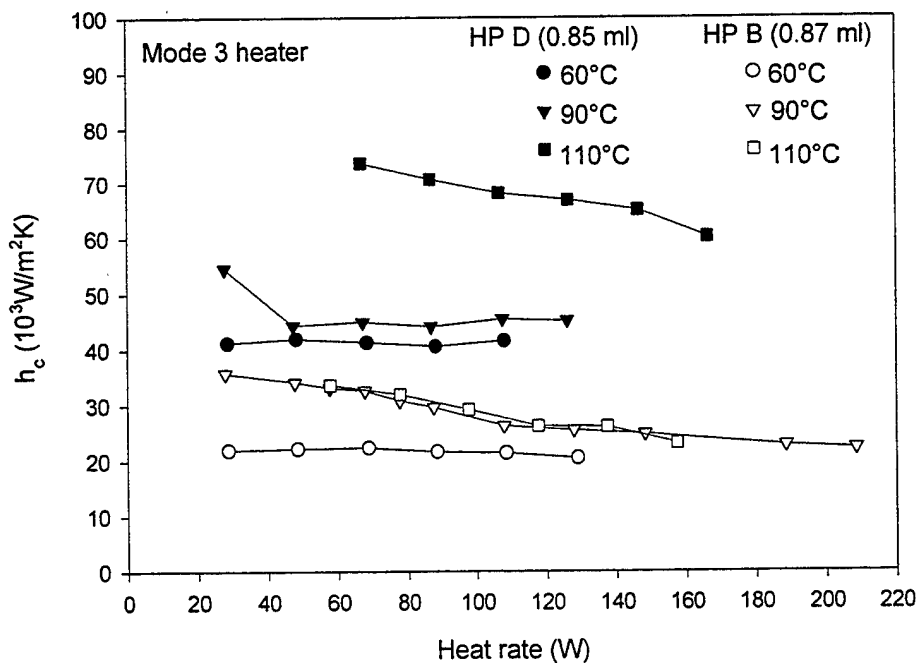

Figure 3.45 Comparison of the heat transfer coefficient of condenser between heat pipe D and heat pipe B at three different operating temperatures for mode 3 heater.

3.4.2.7 Comparison of achievable performances with the predicted maximum performance

The performance limitations of heat pipe B with capillary fins have been predicted for three different heating modes as presented in Figure 2.5, 2.6 and 2.7. The maximum performance is determined by the lowest performance limitation in an interesting temperature range. During the experiment, achievable performances of heat pipe B are obtained. Since heat pipe B is developed to operate at high heat fluxes and the evaporator-to-condenser temperature difference (ΔT_{ec}) becomes high at the high heat fluxes (e.g., greater than 120 W/cm^2), the achievable performance is either limited by the lowest coolant temperature (4°C) or by the cracking temperature of the heater chip (between 160 °C and 170°C). In spite of this difficulty encountered during the experiment, the data of the achievable performance has exhibited the high performance capability of heat pipe B. The achievable performances of heat pipe B are plotted in Figure 3.46 for mode 1 heater and in Figure 3.47 for mode 2 heater along with the predicted performance limitations. It is indicated that the achievable performances are lower than the predicted maximum performance. For a given operating temperature, the actual maximum performance is expected to be higher than the achievable one.
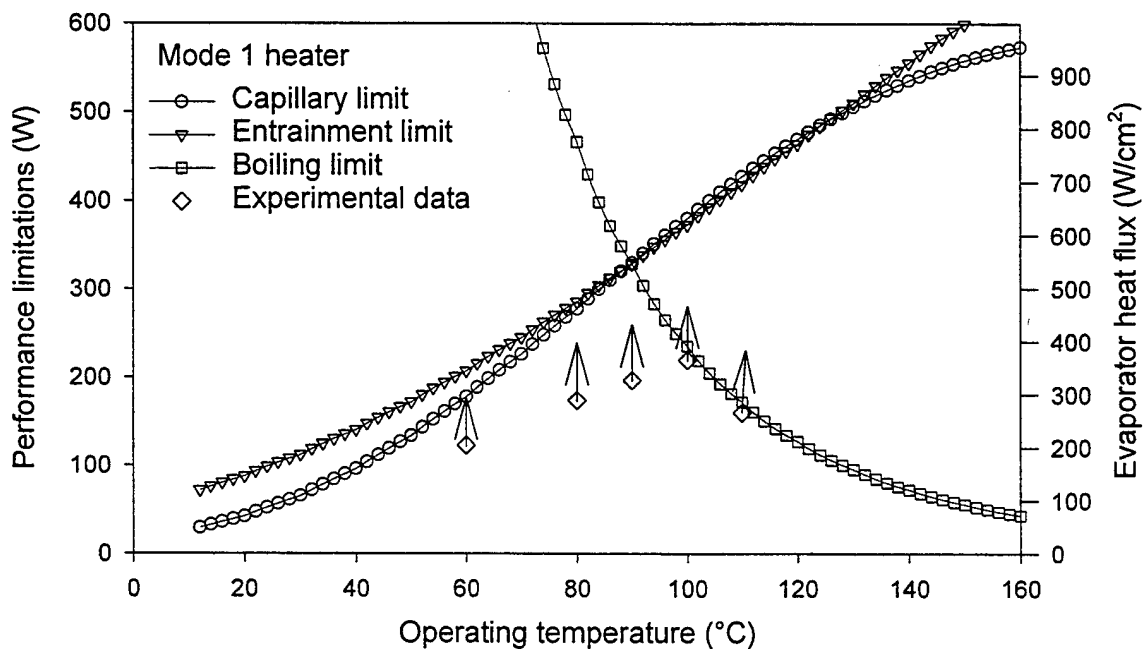

Figure 3.46   Comparison of achievable performances with the predicted maximum performance of heat pipe B with mode 1 heater.
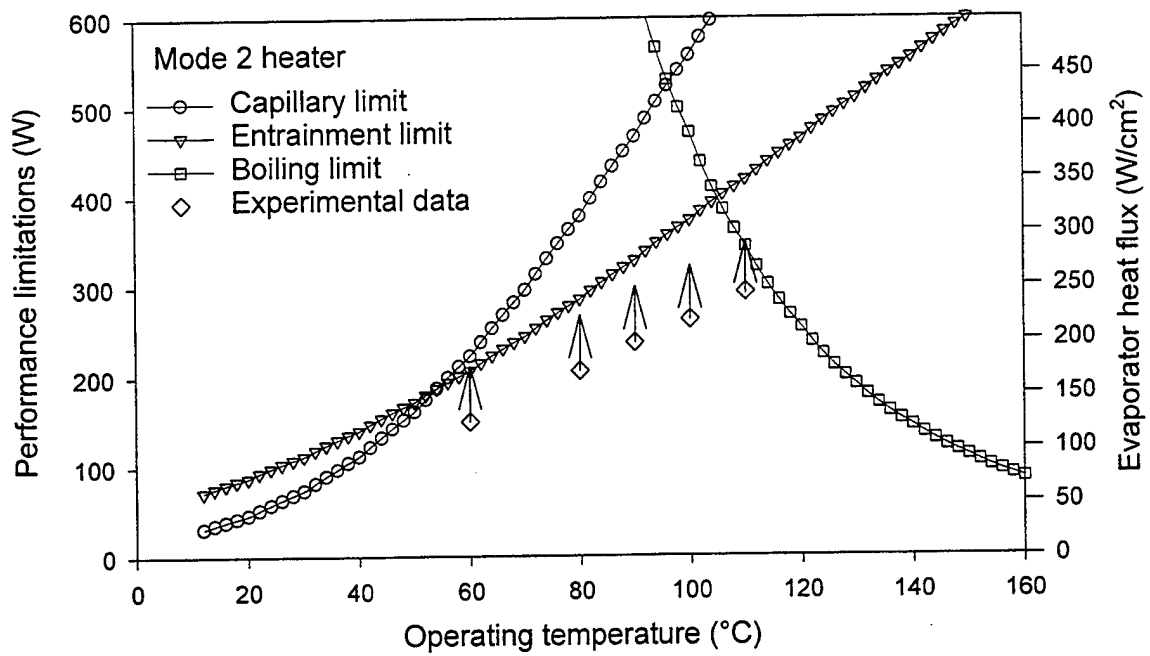
Figure 3.47   Comparison of achievable performances with the predicted maximum performance of heat pipe B with mode 2 heater.

4 CONCLUSIONS AND RECOMMENDATIONS

4.1 Conclusions

Power Division (AFRL/PRP) researchers have developed high performance miniature heat pipes for the cooling of high heat flux electronics using new capillary structures that are made out of a folded copper sheet fin and a folded copper screen. It is easy to make capillary grooves as narrow and deep as desired through the present fabrication techniques. A simple method of assembling the heat pipe with a folded screen has been successfully implemented. Comparisons of the thermal performance for various capillary structures are made. The most efficient and promising capillary structure from the standpoint of heat transfer is the folded copper sheet fins with notches cut in the evaporator and condenser. Achievements of the present investigation are concluded as follows.

◆ Safe operating conditions of the heat pipe are established based on a set of relations describing the four types of heat pipe performance limitations such as the capillary limit, entrainment limit boiling limit and sonic limit. The performance limitations are calculated for the heat pipe with capillary fins using three different heating modes. It is found that at the operating temperature of interest from 40°C to 150°C, the capillary limit, entrainment limit and boiling limit are dominant in three consecutive ranges of the operating temperature. The controlling limitation and its temperature range depend on the evaporator heating configuration.

◆ The capillary pumping heads for the capillary fin and folded screen are qualitatively compared based on Young's equation and magnitudes of the surface tensions of the solid-vapor, liquid-vapor and solid-liquid interfaces. It is derived that the capillary pumping head is higher for the capillary fin than for the folded screen wick.

◆ In the group of folded screen heat pipes, heat pipe G with 1.1 ml fill amount has the best thermal performance. Heat pipe G contains a folded screen wrapped around its inner wall and two stiffeners holding the screen against the heat pipe wall. The fill amount of 1.1 ml corresponds to a fill ratio of 72% (a ratio of the working fluid fill amount to the volume of all the grooves and pores). In comparison, for the group of folded sheet fin heat pipes, the fill amount of 0.87 ml

68

(80% fill ratio) or 0.85 ml (78% fill ratio) results in a better thermal performance.

♦ Though heat pipe D with notches cut in the evaporator and condenser, heat pipe B with capillary fins (without notches), and heat pipe G with screen wick have all demonstrated their favorable thermal performances, heat pipe D has exhibited the lowest internal thermal resistance. Heat pipe B has a lower internal thermal resistance than heat pipe G.

♦ For heat pipe B, the condenser heat transfer coefficient, h_c, decreases slightly with an increase in the heat rate in most cases. Given a heat rate, an increase in the operating temperature results in a slight increase in h_c. Most condenser heat transfer coefficients vary between 19000 W/m²K and 33000 W/m²K. In most cases, the evaporator heat transfer coefficient, h_e, as function of the heat rate has the maximum value for a given operating temperature. The maximum value occurs at a higher heat rate with an increase in the operating temperature.

♦ The ratio of the heat rate through the top side cooler to that through the bottom side cooler of the condenser is defined as the heat rate ratio. The effect of the operating temperature on the heat rate ratio is revealed with heat pipe B. At 80°C, the heat rate ratio decreases from 1.6 to 1.25 with the input power increased from 90 W to 150 W. At 110°C, the heat rate ratio decreases from 1.0 to 0.75 with the input power increased from 80 W to 160 W.

♦ For heat pipe D, the maximum value of h_e is not noticeable for a given operating temperature. With mode 3 heater, the increase in h_e for heat pipe D is varied upward 17% to 95% compared with the case of heat pipe B. Most condenser heat transfer coefficients vary between 40000 W/m²K and 73000 W/m²K, much higher than those of heat pipe B. The condensation heat transfer enhancement is more significant at 110°C. The increase in h_c by 120% or greater for heat pipe D can be achieved at 110°C in comparison with heat pipe B. In heat pipe D, the fin bridges (the uncut part) existing at the top of the folded sheet fin partially separate the liquid flow from the vapor flow and reduce the average counter-current flow shear stress at the liquid-vapor interface. In addition, the fin bridges in the condenser serve as additional secondary heat transfer area. As a result, heat pipe D is superior to heat pipe B in the thermal performance.

♦ The heat pipe thermal performance at high heat fluxes greater than 100 W/cm² is investigated with mode 1 and mode 2 heaters. It has been indicated that the heat transfer coefficients of the evaporator and condenser are still greater for heat pipe D than for heat pipe B at the high heat

69

fluxes. For heat pipe D with mode 2 heater, as an example, the evaporator-condenser temperature difference reaches 36.1°C at an operating temperature of 90°C and a heat flux of 127 W/cm^2, and reaches 34.4°C at 100°C and 141 W/cm^2. Very high heat fluxes are achieved using mode 1 heater with heating area of 0.774 cm^2. During the experiment with the mode 1 heater, no temperature excursion on the evaporator wall of the heat pipe has been found in the operating temperature range between 60°C and 100°C even if the heat flux is increased up to 283 W/cm^2 at 100°C and to 158 W/cm^2 at 60°C. However, the peak evaporator temperature has reached 170.4°C for T_v = 100°C and 112.6°C for T_v = 60°C. Concerning this, the temperature difference between the peak temperature and operating temperature is regarded as a more critical parameter to evaluate the performance of the heat pipe with a small heating area. The price for the operation at the very high heat flux is a resultant large evaporator-condenser temperature difference across the heat pipe length. The objective of developing high performance heat pipes is to reduce their internal thermal resistance at the high heat flux.

4.2 Recommendations

The following recommendations are made for future R&D in this area.

◆ The heat pipe wall material could be replaced with lightweight carbon-carbon composites that lead to weight and cost savings if used for space applications. The thermal conductivity of carbon-carbon composites can be much higher than that of aluminum and copper. The material compatibility of a carbon-carbon composite with heat pipe working fluids should be determined through testing. Advanced coating and bonding technologies are needed to assemble carbon-carbon heat pipes.

◆ Measurements of the capillary pumping head and permeability of the folded screen wick may be performed to further evaluate this kind of capillary structure.

◆ Packaged design of the miniature heat pipe to be applied to the cooling of laser diodes and electronic devices may be carried out.

5 REFERENCES

[1]Katoh, T., Amako, K., and Akachi, H., "New Heat Conductor for Avionics Cooling," 11th Int. Heat Pipe Conference, Tokyo, 1999.

[2]   Leland, J. E., "The Effects of Channel Curvature and Protrusion Height on Nucleate Boiling and the Critical Heat Flux of a Simulated Electronic Chip," WL-TR-94-2051, Final Report, Wright Laboratory, AFMC, WPAFB, 1994.

[3]   Peterson, G. P., "An Introduction to heat Pipes," John Wiley & Sons, Inc., New York, 1994.

[4]   Faghri, A., "Heat Pipe Science and Technology," Taylor & Francis, London, 1995.

[5]   Polasek, F., and Zelko, M., "Thermal Control of Electronic Components by Heat Pipes and Thermosyphons," 10th Int. Heat Pipe Conference, Stuttgart, 1997.

[6]   Plesch, D., Bier, W., Seidel, D., and Schubert, K., "Miniature Heat Pipes for Heat Removal from Microelectronic Circuits," ASME Annual Meeting, Altanta, 1991.

[7]   Cao, Y., Gao, M., Beam, J. E., and Donovan, B., "Experiments and Analyses of Flat Miniature Heat Pipes," 31th Intersociety Energy Conversion Engineering Conference, Washington, DC, 1996.

[8]   Faghri, A., and Khrustalev, D., "Micro/Miniature Heat Pipe Technology for Electronic Cooling," WL-TR-97-2083, Final Report, Wright Laboratory, AFMC, WPAFB, 1997.

[9]   Ponnappan, R., "A Novel Micro-capillary Groove-wick Miniature Heat Pipe," AIAA 2000-2947, 35th Intersociety Energy Conversion Engineering Conference, Las Vegas, 2000.

[10]   Groll, M., Roesler, S., and Lin, L., "Investigation of Vertical High-performance Closed Two-phase Thermosyphons with Perforated Tube Flow Separators," Int. Symposium on Phase Change Heat Transfer, Chongqing, P. R. China, 1988.

[11]   Hopkins, R., Faghri, A., and Khrustalev, D., "Flat Miniature Heat Pipes with Micro Capillary Grooves," Journal of Heat Transfer, Vol. 121, No. 1, 1999, pp.102-109.

[12]   Tien, C. L., and Chung, K. S., "Entrainment Limits in Heat Pipes," 3rd Int. Heat Pipe Conference, Palo Alto, California, 1978.

[13]   Chi, S. W., "Heat Pipe Theory and Practice," Hemisphere Publishing, Washington D.C., 1976.

[14]   Grote, M. G., Stark, J. A., and Tefft, E, C., "Enhanced Evaporative Surface for Two-Phase Mounting Plates," 16th ICES Conference, Paper No. 860979, 1986.

[15]   Kline, S. J. and McClintock, F. A., "Describing Uncertainties in Single-Sample Experiments," Mechanical Engineering, ASME, January, 1953, pp. 3-8.